Variations in eastern Mediterranean hydrology during the last climatic cycle as inferred from neodymium isotopes in foraminifera

Maxence Duhamel, Christophe Colin, Marie Revel, Giuseppe Siani, Arnaud Dapoigny, Éric Douville, Jiawang Wu, Yulong Zhao, Zhifei Liu, Paolo Montagna

Variations in eastern Mediterranean hydrology during the last climatic cycle as inferred from neodymium isotopes in foraminifera

Maxence Duhamel[1], Christophe Colin[1*], Marie Revel[2], Giuseppe Siani[1], Arnaud Dapoigny[3], Eric Douville[3], Jiawang Wu[4], Yulong Zhao[4], Zhifei Liu[4], Paolo Montagna[5]

1. Université Paris-Saclay, Laboratoire GEOsciences Paris-Sud, GEOPS/IPSL, 91405 Orsay Cedex, France.
2. Université de la Cote d'Azur, CNRS, OCA, IRD, Geoazur, 250 rue Albert Einstein, 06500 Valbonne, France.
3. Laboratoire des Sciences du Climat et de l'Environnement, LSCE/IPSL, CEA-CNRS-UVSQ, Université Paris-Saclay, F-91191 Gif-sur-Yvette, France.
4. State Key Laboratory of Marine Geology, Tongji University, Shanghai 200092, China.
5. ISP-CNR, via Gobetti 101, 40129 Bologna, Italy.

Corresponding author: Christophe Colin – christophe.colin@u-psud.fr

Abstract

The Nd isotopic compositions (εNd) of mixed planktonic foraminifera have been analyzed in two sediment cores collected in the Nile deep-sea fan in order to reconstruct past εNd of the Eastern Mediterranean Deep Water (EMDW) and to assess the relative contributions of Nile discharge and Modified Atlantic Water (MAW) inflow to the Eastern Mediterranean Sea hydrology, as well as their potential control on anoxic events over the last climatic cycle. The two foraminiferal εNd records are similar and display a increase in εNd values during the African Humid Periods. Superimposed on this precession-forced variability (insolation received by the Earth at low latitudes), the record of variations in foraminiferal εNd indicates a 2-unit decrease in εNd during the interglacial Marine Isotope Stages (MIS) 5 and 1 compared to glacial MIS6, 4, 3 and 2. The εNd results suggest that the long-term glacial to interglacial changes in Nd isotopic composition of EMDW were not entirely induced by variations in Nile River discharge and Saharan dust inputs. Decreases in εNd during MIS5 and MIS1 interglacials indicate an increase in the contribution of unradiogenic MAW to the eastern Mediterranean Sea related to high sea-level stands and greater seawater exchange between the North Atlantic and Mediterranean basins. In addition, radiogenic

seawater εNd values observed during African Humid Periods (and sapropel events) are associated with an intensification of Nile discharge and an increase in residence time of deep-water masses in the eastern Mediterranean Sea, which induces an increase in the interaction between deep-water masses and radiogenic sediments along the margin of the eastern Mediterranean Sea. Results confirm that an intensification of the hydrological exchanges between the western and eastern Mediterranean basins during high sea-level stand and the subsequent higher proportion of Atlantic Water in the Levantine Basin may have preconditioned the eastern Mediterranean Sea to sapropel depositions during the last climatic cycle.

Key words: *Neodymium isotopes; foraminifera; paleo-hydrology; sapropels; eastern Mediterranean Sea; African monsoon.*

1. Introduction

The Mediterranean Sea is a semi-enclosed basin, where an excess of evaporation over precipitation and runoff induces a characteristic eastward increase in the salinity of the surface Atlantic water that enters through the Gibraltar Strait and flows to the eastern Mediterranean basin; this water effectively becomes denser and contributes to the formation of intermediate and deep waters. The resulting Mediterranean thermohaline circulation has been demonstrated to be highly sensitive to present-day and past climate changes in both high and low latitudes (Rossignol-Strick et al., 1982; Roether et al., 1996; Kallel et al., 1997; Pinardi and Masetti, 2000; Rohling et al., 2002; Emeis et al., 2003; Scrivner et al., 2004; Melki et al., 2009; Revel et al., 2010; Toucanne et al., 2015; Filippidi et al., 2016; Tesi et al., 2017). This variability is thought to be responsible for the deposition of organic-rich sapropel layers (characterized by >1% C_{org}) in the Eastern Mediterranean Sea (EMS) (Murat and Got, 2000) and of Organic Rich Levels (ORL) in the Western Mediterranean Sea (WMS) (e.g. Rohling et al., 2015). However, paleo-hydrological processes and associated ventilation dynamics related to sapropel deposition are still debated because conventional water-mass proxies, such as $\delta^{13}C$ analyzed on benthic foraminifera, cannot be used systematically due to the lack of benthic foraminifera in EMS sediments during time intervals when bottom waters were characterized by anoxic conditions.

Despite many unresolved problems, such as the processes responsible for the sluggish thermohaline circulation during deep-sea anoxic events, significant advances have been made

over recent decades in our understanding of sapropel formation since the pioneering work of Rossignol-Strick et al. (1982). There is now a common consensus that the formation of sapropels in the Mediterranean Sea is closely linked to: (1) reduced deep-water ventilation associated to freshwater input lowering surface water salinity, thus causing stratification of the water masses with limited or no oxygen renewal in deep water; or (2) nutrient-rich surface freshwater inputs, which significantly increase surface productivity and induce the mineralization of organic matter in deep water to a level that exceeds oxygen inputs through deep water mass renewal; or (3) a combination of both processes (Rohling, 1994; Cramp and O'Sullivan, 1999; Rohling et al., 2015). The leading role of stratification in most studied sapropels is revealed by the neodymium (Nd) isotopic composition of biogenic/authigenic fractions (e.g. Freydier et al., 2001; Cornuault et al., 2018; Wu et al., 2019), benthic foraminifera carbon isotopic records, faunal assemblages (e.g. Kuhnt et al., 2008; Schmiedl et al., 2010; Cornuault et al., 2016), redox-sensitive elemental compositions (e.g. Jilbert et al., 2010; Tachikawa et al., 2015; Tesi et al., 2017), and circulation models (e.g. Myers er al., 1998; Myers, 2002; Stratford et al., 2000; Bianchi et al., 2006; Grimm et al., 2015; Vadsaria et al., 2019).

Many studies have confirmed that periods of sapropel deposition are marked by high river runoff originating from the low-latitude monsoonal system, whereas time intervals between sapropel depositions are arid with reduced riverine runoff and increased wind-blown sediment supplies (e.g. Wehausen and Brumsack, 1999; Larrasoaña et al., 2003; Zhao et al., 2012; Revel et al., 2014). A widely accepted explanation for the excess freshwater input during times of sapropel formation is related to heavy monsoonal precipitation in North Africa which was channeled by the Nile River and other North African paleo-rivers (e.g. Rossignol-Strick et al., 1982; Fontugne et al., 1994; Rohling et al., 2002; Emeis et al., 2003; Scrivner et al., 2004; Osborne et al., 2008, 2010; Revel et al., 2010; Wu et al., 2016, 2017). In North Africa, these humid periods have been attributed to the northward migration of the rain belt associated with the Inter-Tropical Convergence Zone (ITCZ) due to precession-driven insolation changes (Rossignol-Strick et al., 1982; DeMenocal et al., 2000; Gasse, 2000; Arbuszewski et al., 2013; Skonieczny et al., 2015, 2019). The last period of more intense rainfall compared to the present, the so-called African Humid Period (AHP: from ~14.8 and ~6 cal kyr BP; Shanahan et al., 2015; Bastian et al., 2017), is thought to be responsible for the formation of the organic-rich sapropel S1 in the EMS between 10.2 and 6.4 cal kyr BP (Mercone et al., 2000; De Lange et al., 2008). Thus, the strong correspondence between sapropel formation and periods of African monsoon intensification, when freshwater discharge by North African rivers

into the Mediterranean Sea increased, suggests that the reduction in sea surface salinity and deep-water convection could be the result of changes in the African monsoon system (Revel et al., 2015; Rohling et al., 2015). However, enhanced freshwater inputs from the northern margin of the Mediterranean Sea related to precipitations driven by westerly winds and the melting of glacial ice-sheets and linked to climate changes in the high latitudes of the Northern hemisphere (e.g. Kallel et al., 1997; Emeis et al., 2003; Melki et al., 2009; Toucanne et al., 2015; Filippidi et al., 2016; Tesi et al., 2017) would have also led to the reduction of deep-water formation in the EMS, limiting the oxygen supply to the deep water (Rohling, 1994). Furthermore, several studies have shown that the Mediterranean thermohaline circulation is sensitive to rapid climatic changes in the northern hemisphere (e.g. Heinrich and Dansgaard - Oeschger events) (Rohling et al., 1995; Kallel et al., 1997; Allen et al., 1999; Bartov et al., 2003; Martrat et al., 2004).

In addition, the narrow and shallow Siculo-Tunisian and Gibraltar Straits tend to limit exchanges between the eastern and western Mediterranean basins, and with the North Atlantic. It has been proposed that water exchanges through the Straits may have been significantly limited during the glacial low sea-level stands of the late Quaternary. A general circulation model has shown that Mediterranean water outflow was reduced by 50% during the Last Glacial Maximum (LGM) (Mikolajewicz, 2011), and several studies have pointed to a salinity increase in the eastern basin (Thunell and Williams, 1989; Myers et al., 1998a). In particular, Mikolajewicz (2011) has shown that the formation of deep waters in the eastern basin during the LGM was strengthened and that these waters were principally formed in the Aegean Sea and not in the Adriatic Sea as is the case today. It has also been proposed that rising global sea level during deglaciation led to greater exchanges between the basins and a drop in surface salinity, thus preconditioning the sapropel event by slowing down intermediate and deep convections (Grimm et al., 2015).

Studies of past changes in Mediterranean thermohaline circulation have mostly investigated the last glacial period, focusing on the deposition of sapropel S1 (10.2 – 6.4 cal kyr BP; Mercone et al., 2000) (e.g. Cacho et al., 2002; Sierro et al., 2005; Frigola et al., 2008; Schmiedl et al., 2010; Toucanne et al., 2012; Angue Minto'o et al., 2015; Jiménez-Espejo et al., 2015). Continuous $\delta^{13}C$ and $\delta^{18}O$ records from epibenthic foraminifera of the last glacial – interglacial climatic cycle are rare and difficult to obtain for bottom suboxic or anoxic environments (e.g. sapropel events) in the EMS. This is due to the lack of a continuous population of epibenthic foraminifera species for which a calibrated vital effect for $\delta^{13}C$ analyses is well established (Schmiedl et al., 2003, 2010).

Consequently, the hydrological pattern of the EMS is not well constrained for periods of sapropel deposition and for the time intervals that preconditioned such events.

In the present study, we have investigated the Nd isotopic composition (εNd) of the diagenetic Fe-Mn coatings precipitated on foraminifera shells. It has been demonstrated that εNd measured on planktonic foraminifera shells represents mainly bottom seawater and/or pore water εNd (Tachikawa et al., 2013, 2014). Such εNd obtained from foraminiferal shells have been previously used to provide information on water mass provenance and mixing in the ocean (Molina-Kescher et al., 2014; Wu et al., 2015b, 2019; Dubois-Dauphin et al., 2017; Cornuault et al., 2018). Modern Mediterranean seawater displays a wide range of εNd values, from -11 to -5, with unradiogenic surface water entering the Mediterranean as Atlantic Water and more radiogenic intermediate and deep waters originating from the Levantine Basin (Henry et al., 1994; Tachikawa et al., 2004; Vance et al., 2004). With a residence time of 500-1000 years (Tachikawa et al., 2003; Siddall et al., 2008) and distinct local basin-scale sources, εNd is assumed to behave quasi-conservatively, with great potential to fingerprint the provenance of Mediterranean water masses (Dubois-Dauphin et al., 2017; Cornuault et al., 2018; Wu et al., 2019).

The εNd of mixed planktonic foraminifera from two sediment cores collected in the Levantine Basin were investigated in order to reconstruct past εNd of the EMDW over the last 145 kyr. Combined with previous εNd records, the new results allow us to assess the relative contributions of Nile discharge and inflow of Modified Atlantic Water (MAW) to the thermohaline circulation of the EMS over the last climatic cycle characterized by several anoxic events and the deposition of sapropels S1 to S5. This allows us to constrain the hydrology at the origin of these anoxic events under different environmental conditions (different sea levels, different freshwater supplies from the African rivers and different hydrological exchange conditions at the Gibraltar and the Siculo-Tunisian Straits).

2. Regional hydrological setting in terms of εNd

The Mediterranean Sea is an almost enclosed basin that exchanges surface and intermediate waters with the Atlantic Ocean though the Gibraltar Strait (sill depth ~ 300 m) and surface water with the Black Sea through the Dardanelles Strait (sill depth ~100 m). Driven by a negative water budget, an anti-estuarine circulation occurs in the Mediterranean Sea. Hence, the relatively fresh surface Atlantic Water (AW) (salinity ~ 36.5), which has an unradiogenic εNd signature of ~-9.7 (Tachikawa et al., 2004), flows into the WMS and is then modified by mixing with the ambient

surface water to reach ~-10.4 in the Alboran Sea (Tachikawa et al., 2004, Spivack and Wasserburg, 1988). During its eastward flow, AW mixes with the surrounding surface waters and underlying intermediate waters leading to the formation of the Modified Atlantic Water (MAW) that flows along the basin at 50-200 m water depth following a general cyclonic flow path with several eddies and meanders (Fig. 1). The εNd values for MAW range from -10.8 to -9.0 in the western basin (Henry et al., 1994) and from -9.8 to -4.9 in the eastern basin (Tachikawa et al., 2004; Vance et al., 2004). Since evaporation exceeds precipitation and river runoff, the relatively fresh surface AW flowing into the WMS also becomes progressively saltier (~ 38.5) as it circulates eastward.

During winter time, intense cooling and strong wind-induced heat loss produce denser waters that sink via convection and form the intermediate waters in the Aegean Sea and the Levantine Basin and deep waters in the Gulf of Lions and the Adriatic Sea (Robinson et al., 2001; Schroeder et al., 2012). In particular, the Levantine Intermediate Water (LIW) is formed in the Cyprus-Rhodes area and it spreads westwards throughout the entire Mediterranean Basin at depths of between ~150-700 m (Lascaratos et al., 1993; Malanotte-Rizzoli et al., 1999). The LIW acquires its εNd signature mainly from the partial dissolution of particles from the Nile River and the Egyptian/Libyan margin sediments of the EMS, which have εNd values ranging from -7 to -2 (Weldeab et al., 2002a; Tachikawa et al., 2004; Ayache et al., 2016). This more radiogenic Nd signature is explained by sediment originating from the erosion of Ethiopian traps including Cenozoic basaltic silicate rocks (εNd > 0) (Garzanti et al., 2015). The LIW is thus characterized by a radiogenic εNd of ~-4.8 in the eastern part of the EMS and by an east-west εNd gradient ranging from -4.8 to -9.2, resulting from mixing with overlying and underlying water masses along its path (Henry et al., 1994; Tachikawa et al., 2004; Vance et al., 2004). In the Adriatic Sea, LIW is involved in the formation of Adriatic Deep Water (AdDW) that sinks into the deep EMS contributing, together with the Aegean Deep Water (AeDW), to the formation of the Eastern Mediterranean Deep Water (EMDW). The EMDW εNd values range from -7 to -6 with an average value of -6.5 (Tachikawa et al., 2004). The Western Mediterranean Deep Water (WMDW) is formed in the Gulf of Lions in winter, as a result of mixing between the relatively fresh surface water and the saline LIW; it then spreads into the Balearic Basin and Tyrrhenian Sea between ~ 2000 and ~ 3000 m (Millot, 1999; Schroeder et al., 2012) (Fig. 1). The WMDW is characterized by an average εNd value of -9.4 ± 0.9 (Henry et al., 1994; Tachikawa et al., 2004). Between the WDMW and the LIW (from ~ 700 to ~ 2000 m), the Tyrrhenian Deep Water (TDW) (Millot et al., 2006), which is produced by mixing between WMDW and EMDW, has an average εNd value of -8.1 ± 0.5.

The Blue Nile and Atbara rivers represent together 97% of the suspended sediment load and 68% of the freshwater supply of the total annual Nile discharge (Foucault and Stanley, 1989; Williams et al., 2000; Revel et al., 2015). εNd signatures of sediments from the Nile Basin are characterized by contrasted signatures, ranging from radiogenic values (εNd ≈ 0) for the Cenozoic Ethiopian traps to strongly unradiogenic values (εNd ≈ -30) for the Precambrian Central Africa Craton (Garzanti et al., 2015). Sediments from the Bahr el Jebel (between Lake Albert and 10°N of latitude) are characterized by a εNd value of -25, whereas Victoria-Albert Nile-derived fluvial muds by a range from -29 to -36 (Padoan et al., 2011). The Equatorial-White Nile sediment makes up approximately 3.5 % of the present-day total sediment discharge of the Nile and is fairly constant throughout the year (Blanchet et al., 2015; Garzanti et al., 2015), with a very unradiogenic signature (from -30 to -35). In contrast, the Blue Nile sediment, which is mainly transported during the humid phase, dominates the total sediment discharge of the Nile (72%) and is characterized by very radiogenic εNd values (from -3 to 5; Padoan et al., 2011; Blanchet et al., 2013; Garzanti et al., 2015).

2. Material and methods

2.1 Studied cores

For this study, we have selected cores MD90-964 and MS27PT, which are bathed by the Eastern Mediterranean Deep Water (EMDW).

Core MD90-964 (33°02.75'N, 32°38.57'E; water depth 1375 m, length 32.12 m) was collected on the eastern part of the Nile deep-sea fan during the PROMETE III campaign on board R/V Marion Dufresne in September 1990 (Fig. 1). Core MD90-964 sediments consist of pale cream to yellowish brown foraminiferal and nannofossil marl ooze, interbedded with sapropelic layers that vary in thickness from 2 to 41 cm (Zhao et al., 2011). The $\delta^{18}O$ of *Globigerinoides ruber*, clay mineralogy, total organic carbon (TOC) content and elemental intensities by X-ray fluorescence (XRF) have been studied previously by Zhao et al. (2011). The age model of core MD90-964 (Zhao et al., 2011) has been established by correlating the *G. ruber* $\delta^{18}O$ record and the Mediterranean *G. ruber* stack compiled by Lourens (2004), using Gaussian filtering at both obliquity and precession, and cross-spectral analysis against a target curve that reflects characteristics of orbital parameters (ETP curve). According to the age model, the upper 7.30 m of core MD90-964 investigated in this study cover the last 145 kyr and present a linear mean sedimentation rate of 5 cm/kyr. Sapropels S1, S3,

S4 and S5 are identified by an increase of C_{org} content, which reaches up to 6 % during the deposition of sapropel S5 (Fig. 2; Zhao et al., 2011).

Core MS27PT (31°47.90'N, 29°27.70'E; water depth 1389 m, length 7.3 m) was retrieved on the western Nile delta, around 90 km from the mouth of the Rosetta Nile River, during the Mediflux MIMES cruise of the R/V Pelagia in 2004 (Fig. 1). The core site lies directly under the influence of the Nile freshwater discharge. For this study, we have investigated the upper 3.15 m of core MS27PT which consist of carbonate-rich facies with coarse quartz grains and clastic mud-rich facies where sapropel S1 has been identified (Revel et al., 2010) (Fig. 2). The age model of the studied interval of core MS27PT is based on 22 previously published AMS ^{14}C dates (Revel et al., 2010, 2015; Bastian et al., 2017; Menot et al., 2020) (Fig. 2).

3. Methods

The samples investigated in this study consist of 15 to 30 mg of mono-specific planktonic foraminifera *G. ruber* and mixed planktonic foraminifera, hand-picked in the >150 µm size fraction. Cleaning procedure and purification of Nd have been done in a class 100 clean laboratory using ultrapure reagents. All of the test samples were crushed between two glass slides to open the foraminiferal chambers. The calcite fragments were then ultrasonicated for 1 min before pipetting off the suspended particles with water to separate the waste. This step was repeated until the water became clear and free of clay. All samples were checked under a binocular microscope to ensure that all particles had been removed. Most of the samples were then analyzed after this preliminary physical cleaning step (hereafter referred as "uncleaned foraminifera") (Wu et al., 2015b).

For this study, some physically cleaned samples were transferred to centrifuge tubes for an oxidative-reductive cleaning step (hereafter referred as "cleaned foraminifera"). The oxidative-reductive foraminiferal cleaning procedure followed that described by Vance and Burton (1999), using 10 ml reductive solution (1 M hydrous hydrazine, 16 M NH_4OH, 0.25 M citric acid in a ratio of 1:6:3) and 5 ml oxidative solution (0.2 M NaOH and 30% H_2O_2 in a 1:1 ratio) per sample to more efficiently remove authigenic Fe-Mn coatings and organic material. For the reductive step, samples were heated in a water bath at 80°C for 30 min, and were ultrasonicated every 3 min for 10 s. After transferring the reductive cleaning solution to a centrifuge tube, the cleaned foraminifera were rinsed with Milli-Q water. The analytical procedure for the oxidative step was similar except that samples were ultrasonicated every 10 min for a period of 30 s.

All samples, including uncleaned foraminifera, underwent weak acid leaching for 5 min in 1 ml 0.001 M HNO_3 with ultrasonication. After these cleaning steps, samples were transferred into a 1.5 ml tube. 0.5 ml of Milli-Q water was first added to the tube, and then the foraminifera were dissolved using stepwise 100 µl 0.5 M HNO_3 until the dissolution reaction stopped. The dissolved samples were centrifuged, and the supernatant was immediately transferred to Teflon beakers to prevent leaching of any possible remaining phases. The dissolved foraminifera shell fractions and authigenic fractions contained in the reductive cleaning solution were dried using a hotplate for Nd extraction. Nd was purified using Eichrom TRU-Spec and Ln-Spec resins following the detailed analytical procedures described in Copard et al. (2010). The $^{143}Nd/^{144}Nd$ ratios were measured using the ThermoScientific Neptune^{Plus} Multi-Collector Inductively Coupled Plasma Mass Spectrometer (MC-ICP-MS), hosted at the Laboratoire des Sciences du Climat et de l'Environnement (LSCE) in Gif-sur-Yvette. For the Nd isotope analyses, sample and standard concentrations were matched at 10 ppb. Mass-dependent fractionation was corrected by normalizing $^{146}Nd/^{144}Nd$ to 0.7219 and applying an exponential law. During the analytical sessions, every set of two samples was bracketed by analyses of the La Jolla Nd standard solution, which is characterized by certified values of 0.511858±0.000007 (Lugmair et al., 1983). The offset value between results and certified values of La Jolla standard was lower than 0.4 epsilon units (εNd) for all of the analyses presented in this study. The analytical errors reported herein correspond to the external 2 sigma standard deviation (based on repeated analyses of the La Jolla standard for the different analytical sessions) and range from 0.1 to 0.5 εNd (Table 1 and Table 2). The analytical blank values for Nd evaluated by using a quadrupole ICPMS were <4 pg, which represents less than 0.1% of the minimum Nd yield from foraminifera used in this study. As a result, no blank correction was applied. Results are expressed as $\varepsilon Nd = [(^{143}Nd/^{144}Nd)_{sample}/(^{143}Nd/^{144}Nd)_{CHUR} -1] *10000$, with the present-day $(^{143}Nd/^{144}Nd)_{CHUR}$ of 0.512638 (Jacobsen and Wasserburg, 1980).

4. Results

4.1 The εNd record of cores MS27PT and MD90-964

The εNd values from core MS27PT, obtained on both monospecific samples of planktonic foraminifer *G. ruber* and mixed planktonic foraminifera, exhibit a wide range from -5.71±0.13 to -2.51±0.21 (Table 1 and Fig. 3). The εNd values of monospecific and mixed samples from the same sediment volume are in agreement within an uncertainty of 2 sigma (Table 1). It is worth noting that mean εNd values obtained from foraminifera cleaning solutions are similar or slightly more

radiogenic than cleaned foraminifera. This confirms that oxidative-reductive cleaning procedures applied to foraminiferal tests from our sampling sites are not effective to fully remove the Nd associated with the authigenic Fe-Mn coating (Wu et al., 2015b). Therefore, εNd obtained in both reductively cleaned and non-reductively cleaned foraminifera are associated with bottom and/or pore-water εNd values as it has been demonstrated elsewhere for a large compilation of εNd results obtained from foraminifera (Tachikawa et al., 2014).

For core MS27PT, εNd displays lower values of -4.7±0.2 to -4.9±0.1 between 21 and 16.4 cal kyr BP (Fig. 3). It increases to more radiogenic values (-2.5±0.2 to -4.4±0.3) in the time interval between 14.1 and 6.8 cal kyr BP, corresponding to the AHP which is associated with higher Nile flood discharges (DeMenocal et al., 2000; Revel et al., 2015; Castañeda et al., 2016). The highest value (-2.5±0.2) is recorded at 9.7 cal kyr BP. The εNd values then steadily decrease from -2.5±0.2 to -5.5±0.3 between 9.7 and 4.3 cal kyr BP. The time interval coeval with the period during which sapropel S1 was deposited (10.2-6.4 cal kyr BP) is associated with radiogenic εNd values (from -2.7±0.2 to -4.3±0.2). The time interval between 4.3 and 1.5 cal kyr BP presents unradiogenic εNd values (up to -5.9±0.1) which increase again thereafter to reach -4.0±0.1 at the core top.

For core MD90-964, εNd values were obtained for samples of uncleaned mixed foraminifera from the Marine Isotope Stage (MIS) 6 to the Holocene (Fig. 4E). In general, glacial MIS6, MIS4, MIS3 and MIS2 are characterized by high εNd values, ranging from -3.8±0.2 to -2.8±0.2. In contrast, interglacial MIS5 and the Late Holocene display lower εNd values, from -4.5±0.2 to -2.8±0.3. Superimposed on this long-term glacial-interglacial variation, the monsoon–precession induced signal is distinguished by more radiogenic values related to the African Humid Periods (from 123.5 to 121.7 cal kyr BP, 102.3 to 99.3 cal kyr BP, 84.3 to 81.8 cal kyr BP; 55 cal kyr BP and 9.5 to 6.2 cal kyr BP) (e.g. Gasse, 2000; Zhao et al., 2012). These time intervals are also associated with an increase of C_{org} in core MD90-964 and are coeval with the deposition of sapropels S5 (128.0 to 117.7 cal kyr BP), S4 (102.3 to 100.6 cal kyr BP), S3 (81.8 to 79.7 cal kyr BP) and S1 (10.1 to 5.7 cal kyr BP) (Fig. 4F) (Zhao et al., 2011). In particular, εNd values systematically increase before the deposition of sapropels S4, S3 and S1.

For the last 20 cal kyr BP, the εNd record obtained on core MD90-964 displays long-term variations that are consistent with those of core MS27PT. Interestingly, higher εNd values from ~14 to ~6 cal kyr BP are coeval with the timing of the AHP (Fig. 3). The time interval between 9 and 6 cal kyr BP is marked by a steady decrease of εNd during the Late Holocene (Fig. 3), whereas the

interval between 4 and about 1.5 cal kyr BP displays lower values before they increase again during the last 1.5 cal kyr BP.

4.2 Regional compilation of seawater εNd of the Levantine Basin

Previous studies of the Nd isotopic compositions of authigenic oxy-hydroxides in the Levantine Basin have been conducted on leached bulk sediment (Freydier et al., 2001; Cornuault et al., 2018; Wu et al., 2019), fish debris/teeth (Wu et al., 2019) and on planktonic foraminifera (Scrivner et al., 2004; Vance et al., 2004; Osborne et al., 2010; Cornuault et al., 2018; Wu et al., 2019). Past seawater εNd has been obtained from bulk sediment leachates using different analytical procedures such as bulk sediment leached with 1 M HCl (Freydier et al., 2001; Wu et al., 2019) and hydroxylamine hydrochloride of non-decarbonated samples (Tachikawa et al., 2004; Cornuault et al., 2018). εNd analyses of foraminifera have previously been conducted on both uncleaned foraminifera (Cornuault et al., 2018) and samples treated with an oxidative-reductive leaching procedure (Scrivner et al., 2004; Vance et al., 2004; Osborne et al., 2010). All of these analytical procedures have been debated within the scientific community and have been deemed suitable for extracting the εNd signature of the deep-water masses of the ocean.

Previous εNd records based on cleaned foraminifera collected in the eastern Levantine Basin (ODP Site 967C - 34°04.270'N; 32°43.528'E; 2552.8 m; Scrivner et al., 2004), in the western Levantine Basin (OPD Site 971A - 33°42.818'N; 24°42.108'E; 2140.9 m; Osborne et al., 2008) and in the south-eastern Aegean Sea (core LC21 - 35°39.7'N; 26°35.0'E; 1520 m; Osborne et al., 2010) were used to reconstruct past εNd of surface waters. However, it has been recently demonstrated that εNd of fossil planktonic foraminifera is not related to the ambient seawater at calcification depths, but instead reflects bottom and/or pore-water εNd values due to the presence of residual authigenic Fe-Mn coatings precipitated onto the carbonate shells that cannot be removed by chemical cleaning procedures (Piotrowski et al., 2012; Roberts et al., 2012; Wu et al., 2015b; Xu et al., 2018). εNd results obtained from cleaned foraminifera of core LC21 and ODP sites 967C and 971A should be interpreted as bottom/pore water εNd.

ODP Site 967C is also located within the EMDW (2551 m) and about 100 km away from core MD90-964 making it possible to directly compare their εNd records for time intervals corresponding to sapropels S1 and S5 (Figs. 5 and 6). εNd records for core MD90-964 and Site 967C, display more radiogenic values during African Humid Periods than before and after these time intervals. For core MD90-964, the highest εNd value is observed in the early African Humid

Period (at 13.2 cal kyr BP) before the deposition of sapropels S1. Except this highest εNd value, both sapropels of core MD90-964 (S5 and S1) display a range from -3.5±0.2 to -4.8±0.2, characterized by slightly more radiogenic values compared to those obtained in the ODP Site 967C (-5.5±0.5 to -3.1±0.2; Scrivner et al., 2004).

For the last 20 cal kyr BP, core MS27PT is also characterized by similar long-term variations of εNd with an interval of more radiogenic values between 14 and 6 cal kyr BP followed by a progressive return to unradiogenic values from 6 to 4 cal kyr BP. For cores MS27PT and MD90-964, the last about 1.5 cal kyr BP show more radiogenic values. The good agreement observed in the long-term changes of the εNd during the S5 (for core MD909-964 and ODP Site 967C) and the last 18 cal kyr BP (for core MS27PT, core MD909-964 and ODP Site 967) suggests that all these cores provide a regional Nd isotopic signature of the EMDW.

Core MD04-2722 located south of Cyprus at 1780 m water depth in the eastern Levantine Basin (Fig. 1) presents radiogenic LGM εNd values (around -3), comparable to those observed for cores located along the Nile deep-sea fan. εNd values decrease between 17.5 and 15 cal kyr BP followed by a time interval characterized by radiogenic isotopic composition between 14.5 and 5 cal kyr BP (Fig. 5). The time interval thereafter (between 5 and 3 cal kyr BP) is associated with a slight decrease in the εNd values. Such long-term variations in εNd are quite similar to those observed in cores MD90-964 and MSPT27 located upstream of the general counterclockwise deep-sea circulation of the eastern Mediterranean basin (Fig. 1). Superimposed on this long-term trend, core MD04-2722 is characterized by shifts of εNd to unradiogenic values around 13.5 and 6.8 cal kyr BP that are not observed in other εNd records of the Levantine Basin (MD90-964, MS27PT and ODP Site 967C), with the exception of one shift to a single unradiogenic value at 6.8 cal kyr BP which is also observed in the ODP Site 967C (Fig. 5). This may reflect different time resolutions or a potential local effect on Nd isotopic signature. This implies that long-term variations of εNd below approximatively 1300 m water depth reflect a regional εNd signal of the Levantine Basin. We note a slight decrease of the εNd range along the north-eastward circulation pattern of the deep-water masses that could be the result of a slight modification of the Nd isotopic signature of deep-water masses through lithogenic Nd input from the volcanic margin of the eastern Levantine Basin.

In contrast, the εNd record of core BC07, located closer to core MD90-964 and at shallower depth (893 m), displays variations from -6.2±0.3 to -4.2±0.3 (Freydier et al., 2001) that differ somewhat from those of ODP Site 967C and core MD90-964 during the AHP (Fig. 5). While time intervals

before 15 cal kyr BP and after 6 cal kyr BP are characterized by similar εNd variations as ODP Site 967C and cores MD90-964 and MS27PT, the AHP is instead associated with more unradiogenic εNd, with values as low as -5.9±0.3 during the sapropel S1. This suggests that the εNd record of water masses at ~900 m differs from those obtained at greater water depths (below ~1300 m) for a time interval between 14 and 6 cal kyr BP. The difference between εNd records above and below ~1300 m reaches its maximum during the time interval of sapropel S1 deposition.

5. Discussion

The εNd record obtained from uncleaned foraminifera of core MD90-964 allows us to establish, for the first time, the Nd isotopic signature of the EMDW of the Levantine Basin over the last climatic cycle and to extend our knowledge of the εNd variability for sapropels S1 and S5 to those of S3 and S4. The εNd record of core MD90-964 also displays glacial-interglacial variability with more radiogenic values during glacial MIS (Fig. 4).

A prerequisite for interpreting such seawater εNd variations through time is the characterization of present-day Nd isotopic composition of the main water masses circulating in the eastern Mediterranean basin. Thus, we can evaluate potential temporal changes in the εNd of the end-members during the last climatic cycle, and assess the potential influences of lithogenic Nd input and regional "boundary exchange" on εNd of deep-water masses.

5.1 Possible impact of changes in lithogenic Nd input on the εNd of the Eastern Mediterranean Deep Water in the Levantine Basin

At the present time, the EMS is characterized by contrasting seawater εNd values (~-10 to -5) with strong zonal and vertical gradients which are attributed to a mixing between the inflowing MAW (~-10) and the more radiogenic underlying LIW (~-5) and EMDW (~-6.5) (Tachikawa et al., 2004) (Fig 1b). The latter acquires its εNd signature from boundary exchange with radiogenic basaltic material originating from the Ethiopian traps, which is transported to the EMS by the Nile river (εNd = -3 to +3, Tachikawa et al., 2004), and from the volcanic arc of the Aegean Sea (εNd ~-2.5), with the most radiogenic material being located at the eastern border of the Levantine Basin (εNd = +3.5 to +6) (Ayache et al., 2016).

In this regard, previous studies have explored past variations of seawater εNd in the Levantine Basin as a balance between unradiogenic aeolian Saharan dust and radiogenic Nile river discharge (Scrivner et al., 2004; Revel et al., 2015; Cornuault et al., 2018; Wu et al., 2019), including the

possibility of a significant contribution from paleo-rivers along the African margin (Osborne et al., 2010), or a predominant contribution through the mechanism of boundary exchange (Ayache et al., 2016; Vadsaria et al., 2019; Wu et al., 2016). Tachikawa et al. (2004) have suggested that the Nd flux from Nile River freshwater has a minor influence on the present-day Mediterranean seawater εNd, with its Nd concentration being low and the water input 10 times smaller than the unradiogenic AW flowing from the Western Basin to the shallow waters of the Levantine Basin. Several previous studies have demonstrated that detrital material in the Nile deep-sea fan results from the mixing of sediments derived from Saharan/Libyan dusts and Nile sediments (Weldeab et al., 2002a; Scheuvens et al., 2013; Garzanti et al., 2015; Revel et al., 2015). Cores MD90-964 and MS27PT, located on the Nile deep-sea fan, are then suitable for assessing lithogenic Nd input to the EMDW.

5.1.1 Contribution of the Nile river

Past humid periods, corresponding to the sapropels, were systematically accompanied by higher deposition of iron/smectite-rich sediments in the Nile deep-sea fan, reflecting enhanced physical erosion and transport of sediments from the Ethiopian Highlands (Krom et al., 1999, 2002; Weldeab et al., 2002b; Revel et al., 2010, 2014, 2015; Langgut et al., 2011; Zhao et al., 2012). In contrast, past arid periods are associated with a lower contribution from the Blue Nile and a higher relative proportion of sediments derived from the White Nile, along with a peak in the aeolian dust component (Revel et al., 2015; Zhao et al., 2012). Large smectite contents recorded in cores MD90-964 (Zhao et al., 2012) (Fig. 4D) and MS27PT, combined with Sr and Nd isotopic compositions (Revel et al., 2014) indicate the dominant contribution of the Blue Nile (smectite) to the Nile discharge, at least during the last climatic cycles. The low proportion of sediment derived from the White Nile is mainly due to the Sudd marshes in Southern Sudan which efficiently trap sediments from tributaries of the White Nile (Padoan et al., 2011; Garzanti et al., 2015). In addition, during the African Humid Periods, it has been suggested that large lakes formed in the region extending from Sudd to the confluence at Khartoum (Barrows et al., 2014). These lakes likely further limited the northward transport of unradiogenic Nd sediments to the Nile deep-sea fan. Thus, there is no argument to support the hypothesis that changes in the relative contribution of the Equatorial-White Nile and Blue Nile tributaries triggered the seawater εNd variations observed in cores MD90-964 and MSPT27.

5.1.2 Contribution of African dust

The Saharan dust transported to the EMS is characterized by an unradiogenic εNd values (-15 to -11; Padoan et al., 2011; Scheuvens et al., 2013), potentially contributing to the unradiogenic Nd isotopic signature of surface and intermediate water masses (e.g. Tachikawa et al 2004; Ayache et al., 2016). However, the present-day distribution of εNd in the surface and intermediate water masses of the Mediterranean Sea is mainly attributed to the mixing of the AW and the LIW and suggests a negligible contribution of Nd lithogenic input from aeolian dusts (Wu et al., 2019).

In addition, core MD90-964, located at a distal position on the deep-sea fan, is characterized by lower mean sedimentation rates (5 cm/kyr) compared to core MS27PT (12 cm/kyr) and may be associated with a higher proportion of Saharan dust components. Variations in the mineralogical ratio of smectite/illite obtained on the clay fraction of core MD90-964 have been used to track the relative proportions of Saharan dust (characterized by high illite contents) and Nile contributions (dominated by smectite, 90%, derived from the Blue Nile and Atbara River draining the Ethiopian Plateau flood basalts) (Zhao et al., 2011) (Fig. 4D). The transport of Saharan dust to the Levantine Basin, reconstructed from the smectite/illite ratio, displays slight glacial-interglacial variations with elevated dust inputs during glacial periods. Such results are in agreement with previous studies reporting an increase in dust input to the Mediterranean Sea during this time span induced by the southward migration of the ITCZ (Weldeab et al., 2002b; Revel et al., 2010; Ehrmann et al., 2016, 2017; Lamb et al., 2018) (Fig. 4D). Such glacial increases of unradiogenic εNd dust inputs to the eastern Mediterranean Basin do not appear to have significantly modified the seawater εNd record obtained in core MD90-964, since glacial periods (MIS6 and MIS2-4) are systematically associated with more radiogenic εNd values than those of interglacial periods (MIS5 and MIS1) (Figs. 4D and 4E).

In addition, the seawater εNd record obtained in core BC07, which was collected at a shallower depth (893 m), could have been slightly more affected by the dissolution of Saharan dust relative to the other deeper cores. Such higher contribution of dust dissolution in the upper water column has been demonstrated in previous studies (e.g. Ayache et al., 2016). Yet, this core does not exhibit variations in seawater εNd that might have been induced by a glacial increase in dust fluxes. The time interval corresponding to the AHP (from ~14.8 and ~6 cal kyr BP), when a decrease of aeolian dusts has been demonstrated (DeMenocal et al., 2000; Ehrmann et al., 2013), is in fact associated with more unradiogenic εNd (Fig. 5). A negligible contribution of the dissolution of African dust on past seawater εNd since the last glacial period has been also proposed by

Cornuault et al. (2018) and Wu et al. (2019) for several seawater εNd records obtained from cores located between ~800 and ~3400 m water depth in the western part of the EMS.

5.1.3 Contribution of African paleo-rivers

A vast fossil river channel network has been identified in the Libyan Sahara, which was active during African Humid Periods (Rohling et al., 2002). These paleo-rivers carried alteration products originating from basalts of the Tibesti mountains, (εNd = 5 to 7; Allegre et al., 1981). Some lake mollusks analyzed in Wadi Behar Belema and Wadi Quoquin (two of these paleo-rivers) have shown that the freshwater was significantly radiogenic (εNd = -2.2 to -1.8) compared to the Saharan dust (Osborne et al., 2008). Therefore, it has been suggested that these Libyan paleo-rivers contributed an additional source of radiogenic Nd to the eastern Mediterranean Basin during African Humid Periods (Scrivner et al., 2004). Seawater εNd records for core ODP site 971A (proximal to the mouths of these paleo-rivers compared to more distal ODP Site 967C or core LC21), were used to support this hypothesis during sapropel S5 (Osborne et al., 2008, 2010). However, for different reasons, variations in the foraminiferal εNd obtained from cores located in the eastern EMS cannot be entirely explained by changes in the Nd isotopic composition of the water masses induced by lithogenic input from the African paleo-rivers. First, Sr and Nd isotopic signatures of the detrital fraction of sediments close to the mouth of these Libyan paleo-rivers (core CP10BC), have shown maximum sediment discharges during the sapropel S1b time interval (Wu et al., 2016) whereas εNd records display more radiogenic values at the beginning of the AHP (~14.8 cal kyr BP), reaching a maximum at ~13.5 cal kyr BP for core MD90-964 and at ~9.7 cal kyr BP for core MS27PT (Fig. 5). Second, the sapropel time interval in cores MD90-964 and MS27PT, as well as in several cores previously investigated throughout the EMS (Wu et al., 2019), is associated with a continuous decrease in εNd values during the deposition of sapropel S1 indicating a more radiogenic signature for the S1a than for the S1b time interval (Fig. 5). Finally, core CP10, which should be susceptible to a significant influence from the discharge of Libyan paleo-river sediments due to its proximal location does not in fact exhibit any influence on its seawater εNd record (Wu et al., 2019). Therefore, while we cannot fully rule out a local influence of detrital discharge from the Libyan paleo-rivers on seawater εNd, its contribution to Levantine deep-water masses can be considered negligible.

In conclusion, the process of “boundary exchange” between water masses and volcanic sediment along the margin of the eastern and northern Levantine Basin is one of the major sources of

lithogenic Nd to the Mediterranean Sea (Ayache et al., 2016), but neither changes in the inputs of lithogenic Nd from the Nile River nor from the paleo-rivers of the North African margin can explain the glacial-interglacial variability observed in the seawater εNd records of core MD90-964.

5.2 Paleo-hydrological implications of the εNd records during glacial-interglacial transitions and Terminations I and II

The εNd records for the EMS display significant glacial and interglacial variations, ranging from -2.0±0.2 to -4.3±0.2, with more radiogenic values during glacial MIS6, 4, 3 and 2 (Fig. 4) that may have been induced by the result of an increase in the residence time of deep-water masses in the EMS and/or a decrease in the proportion of unradiogenic MAW flowing into the EMS.

Using a regional ocean-atmosphere coupled climate model, Vadsaria et al. (2019) have shown that a reduction in the formation of deep water in the Eastern basin is associated with an increase in deep-water εNd due to a longer interaction between the water masses and the radiogenic sediments along the eastern margins of the EMS (Ayache et al., 2016). However, since the ventilation of the EMDW was enhanced during glacial MIS2, 4 and 6, due to saltier and denser surface water (Thunell and Williams, 1989; Béthoux et al., 1990; Myers et al., 1998a), the more radiogenic εNd values for the EMDW during glacial periods cannot be attributed to a modification of the residence time of deep-water masses. Moreover, several models have shown that exchange between the Atlantic Ocean and the Mediterranean Sea may have been reduced by as much as half during the glacial low sea-level stands, resulting in a higher longitudinal salinity gradient in the Mediterranean Sea (Bryden et al., 1994; Myers et al., 1998b; Mikolajewicz, 2011; Grimm et al., 2015). Periods of glacial low sea level may have caused a 50% reduction in water exchange between the eastern and the western Mediterranean basins through the Sicilo-Tunisian Strait (Mikolajewicz, 2011; Grimm et al., 2015). Consequently, taking into account that glacial periods were associated with enhanced convection of deep water in the EMS, the more radiogenic εNd observed for the glacial EMDW can be attributed to a decrease in the contribution of the Modified Atlantic Water (MAW) to the eastern Mediterranean Basin. In this case, therefore, there is an entrainment of radiogenic εNd surface water to the deep basin at the center of production of deep-water masses. However, we cannot exclude that the decrease in zonal water exchange between the WMS and the EMS during the glacial period favored also a longer contact time between the EMDW and the radiogenic sediment draping the eastern Mediterranean continental

525 margin during this time. This hypothesis would need to be tested further using a regional
526 modeling approach.

527 However, we have tried to estimate the reduction of MAW to the EMS necessary to explain an
528 increase of 1.5 εNd unit observed in core MD90-964 during glacial time relative to the low values
529 of the MIS1 and 5 (out of sapropel and African Humid Periods) using a simple box-model for Nd in
530 the EMS established by Wu et al. (2019). We have used the present-day input of Nile river and
531 dust to the EMS (Nile×1, Dust×1; Fig.5 of Wu et al., 2019). Results suggest that the observed glacial
532 increase of εNd could be attributed to a decrease of MAW by 55 % relative to today. Such
533 variations are likely overestimated as the radiogenic Nd contribution from Nile could have also
534 been reduced during glacial period. Nevertheless, the calculated reduction of MAW inflow into the
535 EMS during glacial low sea-level stands agrees with the 50 % reduction in water exchange
536 between the eastern and the western Mediterranean basins through the Siculo-Tunisian Strait
537 quantified by Mikolajewicz, (2011) for the LGM.

538 The εNd record of core MD90-964 covers the last Terminations I and II. The significant decrease in
539 the εNd value (from -3.2±0.2 to -4.4±0.2) during Termination I begins at around 18 cal kyr BP and
540 is coeval with a similar decrease in $\delta^{13}C$ obtained from benthic foraminifera (Incarbona et al.,
541 2011; Sprovieri et al., 2012; Toucanne et al., 2012; Cornuault et al., 2016) (Fig. 6). The decrease of
542 the εNd during Termination II observed in core MD90-964 is also associated with a decrease of
543 benthic $\delta^{13}C$, which is particularly well marked in the Ionian Basin, close to the Siculo-Tunisian
544 Strait (Incarbona et al., 2011). The decrease in $\delta^{13}C$ obtained on benthic foraminifera has been
545 linked to a reduction in deep-water convection in the Mediterranean Sea, but the influence of an
546 increase in surface productivity cannot be excluded (Incarbona et al., 2011; Cornuault et al., 2016).
547 During both terminations, the decrease in ventilation suggested by the benthic foraminifera $\delta^{13}C$
548 record is not associated with more radiogenic values, as expected if the seawater residence time
549 in the EMS had increased. On the contrary, the εNd record shows a decrease suggesting a higher
550 contribution of unradiogenic AW to the Eastern Basin linked to the rise of the relative sea level
551 and enhanced water mass exchange between the eastern and western Mediterranean basins. The
552 timing of reduced ventilation and increase in Atlantic Water contribution to the eastern
553 Mediterranean basin is consistent with the ocean-biogeochemical model results obtained by
554 Grimm et al. (2015), which indicate that deep-water anoxia requires a long prelude of deep-water
555 stagnation of about 6 kyr, with no particularly strong eutrophication. The timing and duration of

556 the stagnation prelude agree with the mechanisms for ORL1 (organic-rich layer) deposition in the
557 western Mediterranean Sea proposed by Sierro et al. (2005).

558 In particular, the decreases in both benthic $\delta^{13}C$ and εNd before the sapropels S1 and S5 are
559 coeval with the end of Henrich Stadial 1 and 11 (HS1 and HS11), respectively. It has been
560 postulated that an enhanced inflow of less salty seawater in the Mediterranean Sea during the
561 HS1 time interval favored a reduction in deep-water convection in the western basin and caused
562 the ORL1 deposition between 14.5 and 8.2 cal kyr BP (Cacho et al., 2002; Martínez-Ruiz et al.,
563 2003). However, this time interval is still associated with deep-water convection allowing the
564 transfer of unradiogenic εNd from MAW to the EMDW at the center of deep-water production in
565 the EMS. Our new εNd record from core MD90-964 suggests similar mechanisms during
566 Termination II, with a potential reduction in the salinity of the Atlantic Water flowing into the
567 Mediterranean Sea during the HS11 (Kandiano et al., 2014; Jiménez-Espejo et al., 2015; Grant et
568 al., 2016) and an increase in the proportion of MAW in the deep-water masses of the EMS, 5 to 6
569 kyr prior to the deposition of sapropel S5.

570 **5.3 Variability of the EMS during the African Humid Periods**

571 The εNd record of core MD90-964 reveals that African Humid Periods (maximum of summer
572 insolation) of the last climatic cycle are generally associated with more radiogenic εNd values of
573 the EMDW (Fig. 4). The sample from core MS27PT dated at ~9.7 cal kyr BP displays the most
574 radiogenic εNd value (-2.5±0.2), which corresponds to the maximum of summer insolation
575 received by the Earth at 20°N (Figs. 4 and 6). The planktonic foraminifera $\delta^{18}O$ record from core
576 9509, located under the River Nile plume in the southeastern Levantine Basin (Fig. 1) (Almogi-
577 Labin et al., 2009), shows the most negative values (-1‰) at ~9.3 cal kyr BP, suggesting a large
578 input of freshwater from the Nile during this time. Such variations may therefore involve (i) a
579 more efficient exchange of Nd from seawater and river sediment plumes associated with an
580 intensification of the Nile River sediment discharge during the African Humid Periods (Revel et al.,
581 2010; Cornuault et al., 2016) and/or (ii) a longer residence time of water masses in the EMS during
582 time intervals of stratification of the water column that could have led to increased boundary-
583 exchange processes at the continental margin (Lacan and Jeandel, 2005).

584 Recent studies have shown that river sediment discharges can modify the Nd isotopic composition
585 of surrounding water masses (Singh et al., 2012; Chen et al., 2013; Goswami et al., 2014; Osborne
586 et al., 2014; Rousseau et al., 2015; Wu et al., 2015a), as recently observed in the Bay of Bengal for

a water depth greater than 2000 m (Yu et al., 2018). However, the εNd values of core BC07, collected at a shallower water-depth (893 m) in the lower portion of the LIW, are less radiogenic by 2 εNd units during the sapropel S1 time interval relative to the other εNd records available nearby (core MD90-964). This suggests that lithogenic Nd from Nile river sediment plumes did not play a major role in εNd variations of intermediate and deep-water masses in the eastern Mediterranean Basin during the African Humid Period. However, Nile river sediment plumes could partially explain the εNd variations during the deposition of sapropel S1 given that core MS27PT, located closer to the Nile river month, is characterized by higher εNd amplitude compared to what observed in core MD90-964.

Results from the recent regional circulation model developed by Vadsaria et al. (2019), using a five-fold increase in Nile runoff during the deposition of sapropel S1, show more radiogenic εNd values (by 2 εNd units) for the deep-water masses below 1200 m, associated with a sluggish circulation, stagnation of deep water and consequent longer interaction with the surrounding radiogenic margins. This result agrees well with εNd records obtained for sapropels S1 to S5 (cores MS27PT and MD90-964) that display an increase of up to 2.5 εNd units (Figs. 5 and 6). In addition, the less radiogenic values observed in core BC07 during sapropel S1 are also consistent with model results for intermediate waters (near the LIW) (Vadsaria et al., 2019). Modeling outputs have shown a modification of the sea surface circulation pattern favorable to the propagation of unradiogenic western Mediterranean Sea waters into the intermediate waters of the Levantine Basin. The resulting εNd decrease observed at intermediate water depth is related to less vigorous circulation that also induces a reduction of the exchange with high-radiogenic material from the east of the EMS. Consequently, distinct variations of εNd records for intermediate- and deep-waters observed in cores BC07 and MD90-964 during the interval of sapropel S1 deposition are supported by models and suggest deep-water stagnation and less vigorous circulation of the LIW.

The εNd record of core MS27PT shows an increase around 4 kyr before the deposition of sapropel S1 (from 10.5 to 6.5 cal kyr BP, Bar-Matthews et al., 2000). This is in agreement with the recent Nile sediment discharge records that indicate an increasing discharge at ~15 cal kyr BP that could have induced a freshening of the Mediterranean Sea and a slow-down of the circulation (Revel et al., 2010). Our new results allow us to investigate the potential for a time lag between seawater εNd rise and sapropel onset for the previous sapropels S3, S4 and S5. The smectite/illite mineralogical ratio of core MD90-964 (Fig. 4) enables estimating the Nile discharge over the last

climatic cycle (Zhao et al., 2011). This mineralogical ratio increases at about 15 cal kyr BP, in agreement with an intensification of Nile river discharge prior to the deposition of sapropel S1 (Revel at al., 2010). Taking into consideration the relatively low time resolution of the record, similar time lags can be observed between the seawater εNd record and the deposition of sapropels S3 and S4 (Fig. 4). The seawater εNd values systematically increase before the intervals of sapropels deposition but these shifts to more radiogenic values are not always associated with variations in the smectite/illite ratio. The lower time resolution of the εNd record of core MD90-964 around sapropel S5 does prevent us from clearly identifying a similar time lag.

The time interval coeval with sapropel S5 is characterized by lower εNd values relative to those of sapropels S1 and S4, and to a lesser extent to those of sapropel S3. ODP Site 967C, which is at a more distal position relative to the Nile River mouth, also displays comparable εNd values during the S5 mid-point, with slightly less radiogenic values (of about 0.5 εNd units) at the limits of S5 (Fig. 6). African monsoon rainfall has been more intense during the time interval of the S5 deposition than during sapropels S1 or S4 (Bar-Matthews et al., 2000), likely leading to more intense Nile sediment and freshwater discharges. The lower $\delta^{18}O$ *G. ruber* values obtained from core MD90-964 during S5 compared to S1 points to a more significant freshwater discharge from the Nile to the studied site (Fig. 2C). This suggests that the higher contribution of unradiogenic MAW in this period of particularly high relative sea level (Fig. 6A), may have overtaken the influence of an increase in radiogenic Nd from the Nile input and/or of a lesser vigorous deep-water circulation in the EMS during the deposition of sapropel S5. This would explain why the development of sapropel S5 is not related to higher εNd values compared to other sapropels, such as S1 and S4. For sapropel S4, the εNd record may indicate enhanced Nile river discharge, or more likely, a reduction in EMS-WMS exchange induced by lower sea level during MIS5c compared to MIS5e (Fig. 6A). Further modeling studies are needed to estimate the relative contribution of the MAW to the eastern Mediterranean Basin under the environmental conditions prevailing during the different sapropel depositions and particularly during the high sea-level of S5.

6. Conclusions

Based on the foraminiferal εNd record of cores MD90-964 and MS27PT, located in the eastern Levantine Basin, we provide evidence of significant glacial-interglacial variations in the inflow of Atlantic Water to the EMS during the last climate cycle (last 145 kyr). We have demonstrated for the first time that εNd values for the EMDW are systematically associated with more radiogenic

values during glacial Marine Isotope Stages. Such long-term glacial to interglacial variations in εNd values cannot be solely the result of changes in Nile river discharge and Saharan dust inputs. Decreases in εNd values during MIS5 and MIS1 interglacials have been attributed to an increase in the contribution of unradiogenic MAW to the EMS related to high sea-level stands and enhanced seawater exchange between the North Atlantic and the Mediterranean basins. Termination I and II are associated with a decrease in seawater εNd in line with a decrease in the $\delta^{13}C$ obtained from benthic foraminifera, suggesting a sluggish deep-sea ventilation in the EMS related to a higher contribution of Atlantic Water in the EMS through the Siculo-Tunisian Strait during sea-level rise.

Superimposed on this long-term glacial-interglacial variation, a monsoon–precession induced signal is distinguished in εNd records by more radiogenic values related to African Humid Periods (and sapropel events). These periods of radiogenic εNd of the EMDW have been associated with an intensification of Nile discharge and an increase in the residence time of deep-water masses in the EMS, leading to an increase in the contact time between deep-water masses and radiogenic sediments along the continental margin of the EMS.

Overall, our εNd records combined with previous εNd values obtained in the EMS reinforce the hypothesis that a drastic reduction in the hydrological exchanges between the western and eastern Mediterranean basins, and a subsequent higher proportion of Atlantic Water during sea level rise may have preconditioned sapropel deposition in the EMS during the last climatic cycle, as proposed by Grimm et al. (2015).

Acknowledgements

The research leading to this paper was funded by the French National Research Agency under the "Investissements d'avenir" programme (Grant ANR-11-IDEX-0004-17-EURE-0006), the HAMOC Project (Grant ANR-13-BS06-0003) and the INSU LEFE-IMAGO PALMEDS Project. We gratefully acknowledge the support provided by Louise Bordier during Nd isotopic composition analyses. We especially thank Adi Torfstein and an anonymous reviewer for their constructive reviews, which significantly helped to improve this manuscript.

678 **Figure captions:**

679 Figure 1: (A) Bathymetric map of the Mediterranean Sea showing locations of core MD90-964
680 (33°02.75'N; 32°38.57'E; water depth 1375 m, length 32.12 m), core MS27PT (31°47.90'N,
681 29°27.70'E; water depth 1389 m, length 7.3 m) (blue dots) and all the other sites discussed in this
682 study (black dots) (Freydier et al., 2001; Scrivner et al., 2004; Osborne 2008, 2010; Cornuault et al.,
683 2018). The simplified modern Mediterranean water circulation is broadly indicated. Signatures of
684 Nd isotopic composition are displayed for the Nile River and aeolian dust (Grousset et Biscaye,
685 2005; Padoan et al., 2011; Scheuvens et al., 2013). The potential pathways of North-African paleo-
686 rivers are also depicted in light gray (Rohling et al., 2002; Wu et al., 2017). (B) Longitudinal
687 transect of annual mean salinity of the Mediterranean Sea (i.e. the red shading shown in (A); data
688 from WOA13). εNd values are represented by colored dots (Henry et al., 1994; Tachikawa et al.,
689 2004; Vance et al., 2004). The map and section were generated using Ocean Data View software
690 (Schlitzer, 2015).

691 Figure 2: Age models of cores MD90-964 and MS27PT: (A) age-depth curve for core MS27PT
692 (continuous line) interpolated from AMS ^{14}C dates (Revel et al., 2015; Bastian et al. 2017) and (B)
693 age-depth curve for core MD90-964 (dashed line) (Zhao et al., 2011). (C) $\delta^{18}O$ analyzed on
694 planktonic foraminifera *G. ruber* of core MD90-964 (continuous line) and MedStack composite
695 reference (dashed line; Lourens, 2004). (D) Organic carbon concentration of core MD90-964
696 sediment (Zhao et al., 2011). (E) $\delta^{18}O$ analyzed on *G. ruber* of core MS27PT. (F) Organic carbon
697 concentration of core MS27PT sediment. Black triangles correspond to the radiocarbon dates
698 obtained for core MS27PT. The Marine Isotope Stages (MIS) and time intervals of sapropel layers
699 are also reported.

700 Figure 3: (A) Nd isotopic composition (εNd) obtained from foraminifera of core MS27PT: εNd
701 values obtained from cleaning solution of *G. ruber* (solid green triangle), reductively cleaned *G.*
702 *ruber* (solid blue triangle), non-reductively cleaned *G. ruber* (solid red triangle), reductively
703 cleaned mixed planktonic foraminifera (solid blue rectangle), cleaning solution of mixed planktonic
704 foraminifera (solid green rectangle), non-reductively cleaned mixed planktonic foraminifera (solid
705 red rectangle); (B) εNd obtained on non-reductively cleaned mixed planktonic foraminifera (solid
706 black square) of core MD90-964 for the last 23 cal kyr BP. The Marine Isotope Stages (MIS) and
707 time intervals of sapropel S1 and AHP are also reported.

Figure 4: Variations in (A) the Relative Sea Level (RSL) (Grant et al., 2014) and (B) the summer insolation (June and July) received by the Earth at 20°N, calculated using Analyseries software (Paillard et al., 1996) for the last 160 kyr. (C) Variations of the $\delta^{18}O$ obtained from *G. ruber* of core MD90-964 (Zhao et al., 2011); (D) Variations of the smectite/illite ratio of core MD90-964 (Zhao et al. 2011); (E) Variations of the Nd isotopic composition (εNd) obtained from uncleaned mixed planktonic foraminifera of core MD90-964 (this study); (F) Variations of the Total Organic Carbon (wt%) of sediments from core MD90-964 (Zhao et al., 2011). The Marine Isotope Stages (MIS) and time intervals of Sapropel S1 to S5 deposition are also reported.

Figure 5: Comparison between εNd records obtained in this study (cores MD90-964 and MS27PT) and published records for the last 25 kyr. Core MD04-2722: Cornuault et al. (2018); cores BC07: Freydier et al (2001); SL29: Wu et al. (2019); ODP Site 967C: Scrivner et al. (2004).

Figure 6: (A) Variations in Relative Sea Level (RSL) (Grant et al., 2014) and summer insolation (June and July) received by the Earth at 20°N, calculated using Analyseries software (Paillard et al., 1996) for last 160 kyr. (B) εNd record obtained from ODP Site 967C (Osborne et al., 2010); (C) εNd record obtained from non-reductively cleaned mixed planktonic foraminifera of core MD90-964 (this study); (D) εNd record obtained from non-reductively cleaned mixed planktonic foraminifera of core MS27PT (this study); (E) compilation of $\delta^{13}C$ obtained from benthic foraminifera from Mediterranean cores. Records of $\delta^{13}C$ obtained from benthic foraminifera are published as followed: MD04-2722 by Cornuault et al. (2016); MD01-2472 by Toucanne et al. (2012); ODP Site 963 by Incarbona et al. (2011); MD95-2043 by Cacho et al. (2007).

Table captions:

Table 1: Results of Nd isotopic composition obtained from planktonic foraminifera samples from core MS27PT. Nd isotopic composition were obtained from reductively cleaned foraminifera, cleaning solution, or uncleaned foraminifera. Foraminifera are monospecific (*G. ruber*) or multispecific (mixed planktonic foraminifera). The age of sediments have been determined by linear interpolation between 22 AMS ^{14}C dates of foraminifera (Revel et al., 2010, 2015; Bastian et al., 2017; Menot et al., 2020).

Table 2: Results of Nd isotopic composition obtained from planktonic foraminifera samples from core MD90-964. The age of sediments have been obtained by the correlation between the *G.*

738 *ruber* $\delta^{18}O$ record and the Mediterranean *G. ruber* stack compiled by Lourens (2004) (Zhao et al.,
739 2011).

740

741 **References**

742 Allegre, C.J., Dupré, B., Lambert, B., Richard, P., 1981. The subcontinental versus suboceanic
743 debate. Lead-neodymium-strontium isotopes in primary alkali basalts from a shield area, the
744 Ahaggar volcanic suite. Earth Planet Sci Lett 52, 85–92
745 Allen, J.R.M., Huntley, B., Brandt, U., Brauer, A., Hubberten, H., Keller, J., Kraml, M., Mackensen, A.,
746 Mingram, J., Negendank, J.F.W., Nowaczyk, N.R., Oberhänsli, H., Watts, W.A., Wulf, S.,
747 Zolitschka, B., 1999. Rapid environmental changes in southern Europe during the last glacial
748 period. Nature 400, 740–743. https://doi.org/10.1038/23432
749 Almogi-Labin, A., Bar-Matthews, M., Shriki, D., Kolosovsky, E., Paterne, M., Schilman, B., Ayalon, A.,
750 Aizenshtat, Z., Matthews, A., 2009. Climatic variability during the last ~90 ka of the southern
751 and northern Levantine Basin as evident from marine records and speleothems. Quat. Sci. Rev.
752 28, 2882–2896. https://doi.org/10.1016/j.quascirev.2009.07.017
753 Angue Minto'o, C.M., Bassetti, M.A., Morigi, C., Ducassou, E., Toucanne, S., Jouet, G., Mulder, T.,
754 2015. Levantine intermediate water hydrodynamic and bottom water ventilation in the
755 northern Tyrrhenian Sea over the past 56,000 years: New insights from benthic foraminifera
756 and ostracods. Quat. Int. 357, 295–313. https://doi.org/10.1016/j.quaint.2014.11.038
757 Arbuszewski, J.A., Demenocal, P.B., Cléroux, C., Bradtmiller, L., Mix, A., 2013. Meridional shifts of
758 the Atlantic intertropical convergence zone since the Last Glacial Maximum. Nat. Geosci. 6,
759 959–962. https://doi.org/10.1038/ngeo1961
760 Ayache, M., Dutay, J.-C., Arsouze, T., Révillon, S., Beuvier, J., Jeandel, C., 2016. High resolution
761 neodymium characterization along the Mediterranean margins and modeling of εNd
762 distribution in the Mediterranean basins. Biogeosciences Discuss. 1–31.
763 https://doi.org/10.5194/bg-2016-109
764 Bar-Matthews, M., Ayalon, A., Kaufman, A., 2000. Timing and hydrological conditions of Sapropel
765 events in the Eastern Mediterranean, as evident from speleothems, Soreq cave, Israel. Chem.
766 Geol. 169, 145–156. https://doi.org/10.1016/S0009-2541(99)00232-6
767 Bar-Matthews, M., Ayalon, A., Vaks, A., Frumkin, A., 2017. Climate and Environment
768 Reconstructions Based on Speleothems from the Levant. In Y. Enzel & O. Bar-Yosef (Eds.),
769 Quaternary of the Levant: Environments, Climate Change, and Humans (pp. 151-164).
770 Cambridge: Cambridge University Press. doi:10.1017/9781316106754.017
771 Barrows, T.T., Williams, M.A.J., Mills, S.C., Duller, G.A.T., Fifield, L.K., Haberlah, D., Tims, S.G.,
772 Williams, F.M., 2014. A White Nile megalake during the last interglacial period. Geology 42,
773 163–166. https://doi.org/10.1130/G35238.1
774 Bartov, Y., Goldstein, S.L., Stein, M., Enzel, Y., 2003. Catastrophic arid episodes in the Eastern
775 Mediterranean linked with the North Atlantic Heinrich events. Geology 31, 439.
776 https://doi.org/10.1130/0091-7613(2003)031<0439:CAEITE>2.0.CO;2
777 Bastian, L., Revel, M., Bayon, G., Dufour, A., Vigier, N., 2017. Abrupt response of chemical
778 weathering to Late Quaternary hydroclimate changes in northeast Africa. Sci. Rep. 7.
779 https://doi.org/10.1038/srep44231
780 Béthoux, J.P., Gentili, B., Raunet, J., Tailliez, D., 1990. Warming trend in the Western
781 Mediterranean Deep Water. Nature 347, 660–662
782 Bianchi, D., Zavatarelli, M., Pinardi, N., Capozzi, R., Capotondi, L., Corselli, C., Masina, S., 2006.

Simulations of ecosystem response during the sapropel S1 deposition event. Palaeogeography Palaeoclimatology Palaeoecology 235, 265–287
Blanchet, C.L., Contoux, C., Leduc, G., 2015. Runoff and precipitation dynamics in the Blue and White Nile catchments during the mid-Holocene: A data-model comparison. Quat. Sci. Rev. 130, 222–230. https://doi.org/10.1016/J.QUASCIREV.2015.07.014
Blanchet, C.L., Tjallingii, R., Frank, M., Lorenzen, J., Reitz, A., Brown, K., Feseker, T., Brückmann, W., 2013. High- and low-latitude forcing of the Nile River regime during the Holocene inferred from laminated sediments of the Nile deep-sea fan. Earth Planet. Sci. Lett. 364, 98–110. https://doi.org/10.1016/J.EPSL.2013.01.009
Bryden, H.L., Candela, J., Kinder, T.H., 1994. Exchange through the Strait of Gibraltar. Prog. Oceanogr. 33, 201–248. https://doi.org/10.1016/0079-6611(94)90028-0
Cacho, I., Grimalt, J.O., Canals, M., 2002. Response of the Western Mediterranean Sea to rapid climatic variability during the last 50,000 years: a molecular biomarker approach. J. Mar. Syst. 33–34, 253–272. https://doi.org/10.1016/S0924-7963(02)00061-1
Castañeda, I.S., Schouten, S., Pätzold, J., Lucassen, F., Kasemann, S., Kuhlmann, H., Schefuß, E., 2016. Hydroclimate variability in the Nile River Basin during the past 28,000 years. Earth Planet. Sci. Lett. 438, 47–56. https://doi.org/10.1016/j.epsl.2015.12.014
Chen, T.-Y., Stumpf, R., Frank, M., Bełdowski, J., Staubwasser, M., 2013. Contrasting geochemical cycling of hafnium and neodymium in the central Baltic Sea. Geochim. Cosmochim. Acta 123, 166–180. https://doi.org/10.1016/J.GCA.2013.09.011
Copard, K., Colin, C., Douville, E., Freiwald, A., Gudmundsson, G., de Mol, B., Frank, N., 2010. Nd isotopes in deep-sea corals in the North-eastern Atlantic. Quat. Sci. Rev. 29, 2499–2508
Cornuault, M., Tachikawa, K., Vidal, L., Guihou, A., Siani, G., Deschamps, P., Bassinot, F., Revel, M., 2018. Circulation Changes in the Eastern Mediterranean Sea Over the Past 23,000 Years Inferred From Authigenic Nd Isotopic Ratios. Paleoceanogr. Paleoclimatology. https://doi.org/10.1002/2017PA003227
Cornuault, M., Vidal, L., Tachikawa, K., Licari, L., Rouaud, G., Sonzogni, C., Revel, M., 2016. Deep water circulation within the eastern Mediterranean Sea over the last 95 kyr: New insights from stable isotopes and benthic foraminiferal assemblages. Palaeogeogr. Palaeoclimatol. Palaeoecol. 459, 1–14. https://doi.org/10.1016/J.PALAEO.2016.06.038
Cramp, A., O'Sullivan, G., 1999. Neogene sapropels in the Mediterranean: A review. Mar. Geol. 153, 11–28. https://doi.org/10.1016/S0025-3227(98)00092-9
De Lange, G.J., Thomson, J., Reitz, A., Slomp, C.P., Principato, M.S., Erba, E., Corselli, C., 2008. Synchronous basin-wide formation and redox-controlled preservation of a Mediterranean sapropel. Nature Geoscience 1, 606–610
DeMenocal, P., Ortiz, J., Guilderson, T., Sarnthein, M., 2000. Coherent High- and Low-Latitude Climate Variability During the Holocene Warm Period. Science (80-.). 288, 2198–2202. https://doi.org/10.1126/science.288.5474.2198
Dubois-Dauphin, Q., Montagna, P., Siani, G., Douville, E., Wienberg, C., Hebbeln, D., Liu, Z., Kallel, N., Dapoigny, A., Revel, M., Pons-Branchu, E., Taviani, M., Colin, C., 2017. Hydrological variations of the intermediate water masses of the western Mediterranean Sea during the past 20 ka inferred from neodymium isotopic composition in foraminifera and cold-water corals. Clim. Past 13, 17–37. https://doi.org/10.5194/cp-13-17-2017
Ehrmann, W., Schmiedl, G., Beuscher, S., Krüger, S., 2017. Intensity of African Humid Periods Estimated from Saharan Dust Fluxes. PLoS One 12, e0170989. https://doi.org/10.1371/journal.pone.0170989
Ehrmann, W., Schmiedl, G., Seidel, M., Krüger, S., Schulz, H., 2016. A distal 140 kyr sediment record of Nile discharge and East African monsoon variability. Clim. Past 12, 713–727.

https://doi.org/10.5194/cp-12-713-2016
Ehrmann, W., Seidel, M., Schmiedl, G., 2013. Dynamics of Late Quaternary North African humid periods documented in the clay mineral record of central Aegean Sea sediments. Glob. Planet. Change 107, 186–195. https://doi.org/10.1016/J.GLOPLACHA.2013.05.010
Emeis, K.-C., Schulz, H., Struck, U., Rossignol-Strick, M., Erlenkeuser, H., Howell, M.W., Kroon, D., Mackensen, A., Ishizuka, S., Oba, T., Sakamoto, T., Koizumi, I., 2003. Eastern Mediterranean surface water temperatures and δ ^{18} O composition during deposition of sapropels in the late Quaternary. Paleoceanography 18, n/a-n/a. https://doi.org/10.1029/2000PA000617
Filippidi, A., Triantaphyllou, M.V., De Lange, G.J., 2016. Eastern-Mediterranean ventilation variability during sapropel S1 formation, evaluated at two sites influenced by deep-water formation from Adriatic and Aegean Seas. Quaternary Science Reviews 144, 95–106
Fontugne, M., Arnold, M., Labeyrie, L., Paterne, M., Calvert, S.E., Duplessy, J.C., 1994. Paleoenvironment, sapropel chronology and Nile river discharge during the last 20,000 years as indicated by deep-sea sediment records in the eastern Mediterranean. Radiocarbon 34, 75–88.
Foucault, A., Stanley, D.J., 1989. Late Quaternary palaeoclimatic oscillations in East Africa recorded by heavy minerals in the Nile delta. Nature 339, 44–46. https://doi.org/10.1038/339044a0
Freydier, R., Michard, A., De Lange, G., Thomson, J., 2001. Nd isotopic compositions of Eastern Mediterranean sediments: tracers of the Nile influence during sapropel S1 formation? Mar. Geol. 177, 45–62. https://doi.org/10.1016/S0025-3227(01)00123-2
Frigola, J., Moreno, A., Cacho, I., Canals, M., Sierro, F.J., Flores, J.A., Grimalt, J.O., 2008. Evidence of abrupt changes in Western Mediterranean Deep Water circulation during the last 50kyr: A high-resolution marine record from the Balearic Sea. Quat. Int. 181, 88–104. https://doi.org/10.1016/j.quaint.2007.06.016
Garzanti, E., Andò, S., Padoan, M., Vezzoli, G., El Kammar, A., 2015. The modern Nile sediment system: Processes and products. Quat. Sci. Rev. 130, 9–56. https://doi.org/10.1016/J.QUASCIREV.2015.07.011
Gasse, F., 2000. Hydrological changes in the African tropics since the Last Glacial Maximum, in: Quaternary Science Reviews. pp. 189–211. https://doi.org/10.1016/S0277-3791(99)00061-X
Goswami, V., Singh, S.K., Bhushan, R., 2014. Impact of water mass mixing and dust deposition on Nd concentration and εNd of the Arabian Sea water column. Geochim. Cosmochim. Acta 145, 30–49. https://doi.org/10.1016/J.GCA.2014.09.006
Grant, K.M., Rohling, E.J., Bronk Ramsey, C., Cheng, H., Edwards, R.L., Florindo, F., Heslop, D., Marra, F., Roberts, A.P., Tamisiea, M.E., Williams, F., 2014. Sea-level variability over five glacial cycles. Nat. Commun. 5, 5076
Grant, K.M., Grimm, R., Mikolajewicz, U., Marino, G., Ziegler, M., Rohling, E.J., 2016. The timing of Mediterranean sapropel deposition relative to insolation, sea-level and African monsoon changes. Quat. Sci. Rev. 140, 125–141. https://doi.org/10.1016/J.QUASCIREV.2016.03.026
Grimm, R., Maier-Reimer, E., Mikolajewicz, U., Schmiedl, G., Müller-Navarra, K., Adloff, F., Grant, K.M., Ziegler, M., Lourens, L.J., Emeis, K.C., 2015. Late glacial initiation of Holocene eastern Mediterranean sapropel formation. Nat. Commun. 6, 7099. https://doi.org/10.1038/ncomms8099
Henry, F., Jeandel, C., Dupré, B., Minster, J.-F., 1994. Particulate and dissolved Nd in the western Mediterranean Sea: Sources, fate and budget. Mar. Chem. 45, 283–305. https://doi.org/10.1016/0304-4203(94)90075-2
Incarbona, A., Sprovieri, M., Lirer, F., Sprovieri, R., 2011. Surface and deep water conditions in the Sicily channel (central Mediterranean) at the time of sapropel S5 deposition. Palaeogeogr. Palaeoclimatol. Palaeoecol. 306, 243–248. https://doi.org/10.1016/J.PALAEO.2011.04.030

879 Jacobsen, S.B., Wasserburg, G.J., 1980. Sm-Nd isotopic evolution of chondrites. Earth Planet. Sci.
880 Lett. 50, 139–155. https://doi.org/10.1016/0012-821X(80)90125-9
881 Jilbert, T., Reichart, G.J., Aeschlimann, B., Gunther, D., Boer, W., de Lange, G.J., 2010.
882 Climatecontrolled multidecadal variability in North African dust transport to the
883 Mediterranean. Geology 38, 19–22
884 Jiménez-Espejo, F.J., Pardos-Gené, M., Martínez-Ruiz, F., García-Alix, A., van de Flierdt, T.,
885 Toyofuku, T., Bahr, A., Kreissig, K., 2015. Geochemical evidence for intermediate water
886 circulation in the westernmost Mediterranean over the last 20kyrBP and its impact on the
887 Mediterranean Outflow. Glob. Planet. Change 135, 38–46.
888 https://doi.org/10.1016/j.gloplacha.2015.10.001
889 Kallel, N., Paterne, M., Labeyrie, L., Duplessy, J.-C., Arnold, M., 1997. Temperature and salinity
890 records of the Tyrrhenian Sea during the last 18,000 years. Palaeogeogr. Palaeoclimatol.
891 Palaeoecol. 135, 97–108. https://doi.org/10.1016/S0031-0182(97)00021-7
892 Kandiano, E.S., Bauch, H.A., Fahl, K., 2014. Last interglacial surface water structure in the western
893 Mediterranean (Balearic) Sea: Climatic variability and link between low and high latitudes.
894 Glob. Planet. Change 123, 67–76. https://doi.org/10.1016/J.GLOPLACHA.2014.10.004
895 Krom, M.., Cliff, R.., Eijsink, L.., Herut, B., Chester, R., 1999. The characterisation of Saharan dusts
896 and Nile particulate matter in surface sediments from the Levantine basin using Sr isotopes.
897 Mar. Geol. 155, 319–330. https://doi.org/10.1016/S0025-3227(98)00130-3
898 Krom, M.D., Stanley, J.D., Cliff, R.A., Woodward, J.C., 2002. Nile River sediment fluctuations over
899 the past 7000 yr and their key role in sapropel development. Geology 30, 71.
900 https://doi.org/10.1130/0091-7613(2002)030<0071:NRSFOT>2.0.CO;2
901 Lacan, F., Jeandel, C., 2005. Neodymium isotopes as a new tool for quantifying exchange fluxes at
902 the continent–ocean interface. Earth Planet. Sci. Lett. 232, 245–257.
903 https://doi.org/10.1016/j.epsl.2005.01.004
904 Lamb, H.F., Bates, C.R., Bryant, C.L., Davies, S.J., Huws, D.G., Marshall, M.H., Roberts, H.M., 2018.
905 150,000-year palaeoclimate record from northern Ethiopia supports early, multiple dispersals
906 of modern humans from Africa. Sci. Rep. 8, 1077. https://doi.org/10.1038/s41598-018-
907 19601-w
908 Langgut, D., Almogi-Labin, A., Bar-Matthews, M., Weinstein-Evron, M., 2011. Vegetation and
909 climate changes in the South Eastern Mediterranean during the Last Glacial-Interglacial cycle
910 (86 ka): new marine pollen record. Quat. Sci. Rev. 30, 3960–3972.
911 https://doi.org/10.1016/J.QUASCIREV.2011.10.016
912 Larrasoaña, J.C., Roberts, A.P., Rohling, E.J., Winklhofer, M., Wehausen, R., 2003. Three million
913 years of monsoon variability over the northern Sahara. Clim. Dyn. 21, 689–698.
914 https://doi.org/10.1007/s00382-003-0355-z
915 Lascaratos, A., Williams, R.G., Tragou, E., 1993. A mixed-layer study of the formation of Levantine
916 intermediate water. J. Geophys. Res. 98, 14739. https://doi.org/10.1029/93JC00912
917 Lourens, L.J., 2004. Revised tuning of Ocean Drilling Program Site 964 and KC01B (Mediterranean)
918 and implications for the δ sup18sup O, teph.pdf.
919 Lugmair, G.W., Shimamura, T., Lewis, R.S., Anders, E., 1983. Samarium-146 in the Early Solar
920 System: Evidence from Neodymium in the Allende Meteorite. Science (80-.). 222, 1015–1018.
921 https://doi.org/10.1126/science.222.4627.1015
922 Malanotte-Rizzoli, P., Manca, B.B., D'Alcala, M.R., Theocharis, A., Brenner, S., Budillon, G., Ozsoy,
923 E., 1999. The Eastern Mediterranean in the 80s and in the 90s: the big transition in the
924 intermediate and deep circulations. Dyn. Atmos. Ocean. 29, 365–395.
925 https://doi.org/10.1016/S0377-0265(99)00011-1
926 Martínez-Ruiz, F., Paytan, A., Kastner, M., González-Donoso, J.M., Linares, D., Bernasconi, S.M.,

Jimenez-Espejo, F.J., 2003. A comparative study of the geochemical and mineralogical characteristics of the S1 sapropel in the western and eastern Mediterranean. Palaeogeogr. Palaeoclimatol. Palaeoecol. 190, 23–37. https://doi.org/10.1016/S0031-0182(02)00597-7

Martrat, B., Grimalt, J.O., Lopez-Martinez, C., Cacho, I., Sierro, F.J., Flores, J.A., Zahn, R., Canals, M., Curtis, J.H., Hodell, D.A., 2004. Abrupt temperature changes in the Western Mediterranean over the past 250,000 years. Science (80-.). 306, 1762–1765. https://doi.org/10.1126/science.1101706

Melki, T., Kallel, N., Jorissen, F.J., Guichard, F., Dennielou, B., Berné, S., Labeyrie, L., Fontugne, M., 2009. Abrupt climate change, sea surface salinity and paleoproductivity in the western Mediterranean Sea (Gulf of Lion) during the last 28 kyr. Palaeogeogr. Palaeoclimatol. Palaeoecol. 279, 96–113. https://doi.org/10.1016/j.palaeo.2009.05.005

Ménot, G., Pivot, S., Bouloubassi, I., Davtian, N., Hennekam, R., Bosch, D, Ducassou, E., Bard, E., Migeon, S., Revel, M., 2020. Timing and stepwise transitions of the African Humid Period from geochemical proxies in the Nile deep-sea fan sediments. Quaternary Science Reviews 228.

Mercone, D., Thomson, J., Croudace, I.W., Siani, G., Paterne, M., Troelstra, S., Croudace, L.W., Siani, G., Paterne, M., Troelstra, S., 2000. Duration of S1, the most recent sapropel in the eastern Mediterranean Sea, as indicated by accelerator mass spectrometry radiocarbon and geochemical evidence. Paleoceanography 15, 336–347. https://doi.org/10.1029/1999PA000397

Mikolajewicz, U., 2011. Climate of the Past Modeling Mediterranean Ocean climate of the Last Glacial Maximum 7, 161–180. https://doi.org/10.5194/cp-7-161-2011

Millot, C., 1999. Circulation in the Western Mediterranean Sea. J. Mar. Syst. 20, 423–442. https://doi.org/10.1016/S0924-7963(98)00078-5

Millot, C., Candela, J., Fuda, J.-L., Tber, Y., 2006. Large warming and salinification of the Mediterranean outflow due to changes in its composition. Deep Sea Res. Part I Oceanogr. Res. Pap. 53, 656–666. https://doi.org/10.1016/j.dsr.2005.12.017

Molina-Kescher, M., Frank, M., Hathorne, E.C., 2014. Nd and Sr isotope compositions of different phases of surface sediments in the South Pacific: Extraction of seawater signatures, boundary exchange, and detrital/dust provenance. Geochemistry, Geophys. Geosystems 15, 3502–3520. https://doi.org/10.1002/2014GC005443

Murat, A., Got, H., 2000. Organic carbon variations of the eastern Mediterranean Holocene sapropel: a key for understanding formation processes. Palaeogeography, Palaeoclimatology, Palaeoecology 158, 241-257.Myers, P.G., Haines, K., Rohling, E.J., 1998a. Modeling the paleocirculation of the Mediterranean: The Last Glacial Maximum and the Holocene with emphasis on the formation of sapropel S1. Paleoceanography 13, 586–606. https://doi.org/10.1029/98PA02736

Myers, P.G., Haines, K., Rohling, E.J., 1998b. Myers, Haines, Rohling - 1998 - Modeling the paleocirculation of the Mediterranean The Last Glacial Maximum and the Holocene with emphas.pdf.

Myers, P.G., 2002. Flux-forced simulations of the paleocirculation of the Mediterranean. Paleoceanography 17, 1009. Doi:10.1029/2000PA000613.

Osborne, A.H., Haley, B.A., Hathorne, E.C., Flögel, S., Frank, M., 2014. Neodymium isotopes and concentrations in Caribbean seawater: Tracing water mass mixing and continental input in a semi-enclosed ocean basin. Earth Planet. Sci. Lett. 406, 174–186. https://doi.org/10.1016/j.epsl.2014.09.011

Osborne, A.H., Marino, G., Vance, D., Rohling, E.J., 2010. Eastern Mediterranean surface water Nd during Eemian sapropel S5: monitoring northerly (mid-latitude) versus southerly (sub-

tropical) freshwater contributions. Quat. Sci. Rev. 29, 2473–2483.
Osborne, A.H., Vance, D., Rohling, E.J., Barton, N., Rogerson, M., Fello, N., 2008. A humid corridor across the Sahara for the migration of early modern humans out of Africa 120,000 years ago. Proc. Natl. Acad. Sci. 105, 16444–16447.
Padoan, M., Garzanti, E., Harlavan, Y., Villa, I.M., 2011. Tracing Nile sediment sources by Sr and Nd isotope signatures (Uganda, Ethiopia, Sudan). Geochim. Cosmochim. Acta 75, 3627–3644. https://doi.org/10.1016/J.GCA.2011.03.042.
Paillard, D., Labeyrie, L., Yiou P., 1996. Analyseries 1.0: A Macintosh software for the analysis of geographical timeseries. Eos Trans. AGU, 77, 379.
Pinardi, N., Masetti, E., 2000. Variability of the large scale general circulation of the Mediterranean Sea from observations and modelling: a review. Palaeogeography Palaeoclimatology Palaeoecology 158, 153–174.
Piotrowski, A.M., Galy, A., Nicholl, J.A.L., Roberts, N., Wilson, D.J., Clegg, J.A., Yu, J., 2012. Reconstructing deglacial North and South Atlantic deep water sourcing using foraminiferal Nd isotopes. Earth Planet. Sci. Lett. 357–358, 289–297. https://doi.org/10.1016/J.EPSL.2012.09.036
Revel, M., Colin, C., Bernasconi, S., Combourieu-Nebout, N., Ducassou, E., Grousset, F.E., Rolland, Y., Migeon, S., Bosch, D., Brunet, P., Zhao, Y., Mascle, J., 2014. 21,000 Years of Ethiopian African monsoon variability recorded in sediments of the western Nile deep-sea fan. Reg. Environ. Chang. 14, 1685–1696. https://doi.org/10.1007/s10113-014-0588-x
Revel, M., Ducassou, E., Grousset, F.E.E., Bernasconi, S.M.M., Migeon, S., Revillon, S., Mascle, J., Murat, A., Zaragosi, S., Bosch, D., 2010. 100,000 Years of African monsoon variability recorded in sediments of the Nile margin. Quat. Sci. Rev. 29, 1342–1362. https://doi.org/10.1016/j.quascirev.2010.02.006
Revel, M., Ducassou, E., Skonieczny, C., Colin, C., Bastian, L., Bosch, D., Migeon, S., Mascle, J., 2015. 20,000 years of Nile River dynamics and environmental changes in the Nile catchment area as inferred from Nile upper continental slope sediments. Quat. Sci. Rev. 130, 200–221. https://doi.org/10.1016/J.QUASCIREV.2015.10.030
Roberts, N.L., Piotrowski, A.M., Elderfield, H., Eglinton, T.I., Lomas, M.W., 2012. Rare earth element association with foraminifera. Geochim. Cosmochim. Acta 94, 57–71. https://doi.org/10.1016/j.gca.2012.07.009
Robinson, A.R., Leslie, W.G., Theocharis, A., Lascaratos, A., 2001. Mediterranean sea circulation. Ocean Curr. 1, 19.
Roether, W., Manca, B.B., Klein, B., Bregant, D., Georgopoulos, D., Beitzel, V., Kovacevic, V., Luchetta, A., 1996. Recent changes in eastern Mediterranean deep waters. Science 271, 333–335
Rohling, E.J., 1994. Review and new aspects concerning the formation of eastern Mediterranean sapropels. Mar. Geol. 122, 1–28. https://doi.org/10.1016/0025-3227(94)90202-X
Rohling, E.J., Cane, T.R., Bouloubassi, I., Kemp, A.E.S., Kroon, D., Schiebel, R., Lorre, A., Emeis, K.C., Cooke, S., Jorissen, F.J., Sprovieri, M., 2002. African monsoon variability during the previous interglacial maximum, Earth and Planetary Science Letters. https://doi.org/10.1016/s0012-821x(02)00775-6
Rohling, E.J., Den Dulk, M., Pujol, C., Vergnaud-Grazzini, C., 1995. Abrupt hydrographic change in the Alboran Sea (western Mediterranean) around 8000 yrs BP. Deep Sea Res. Part I Oceanogr. Res. Pap. 42, 1609–1619. https://doi.org/10.1016/0967-0637(95)00069-I
Rohling, E.J., Marino, G., Grant, K.M., 2015. Mediterranean climate and oceanography, and the periodic development of anoxic events (sapropels). Earth-Science Rev. 143, 62–97. https://doi.org/10.1016/j.earscirev.2015.01.008

Rossignol-Strick, M., Nesteroff, W., Olive, P., Vergnaud-Grazzini, C., 1982. After the deluge: Mediterranean stagnation nd sapropel formation. Nature 285, 105–110. https://doi.org/10.1038/295105a0

Rousseau, T.C.C., Sonke, J.E., Chmeleff, J., van Beek, P., Souhaut, M., Boaventura, G., Seyler, P., Jeandel, C., 2015. Rapid neodymium release to marine waters from lithogenic sediments in the Amazon estuary. Nat. Commun. 6, 7592. https://doi.org/10.1038/ncomms8592

Scheuvens, D., Schütz, L., Kandler, K., Ebert, M., Weinbruch, S., 2013. Bulk composition of northern African dust and its source sediments — A compilation. Earth-Science Rev. 116, 170–194. https://doi.org/10.1016/j.earscirev.2012.08.005

Schmiedl, G., Kuhnt, T., Ehrmann, W., Emeis, K.-C.C., Hamann, Y., Kotthoff, U., Dulski, P., Pross, J., 2010. Climatic forcing of eastern Mediterranean deep-water formation and benthic ecosystems during the past 22 000 years. Quat. Sci. Rev. 29, 3006–3020. https://doi.org/10.1016/j.quascirev.2010.07.002

Schmiedl, G., Mitschele, A., Beck, S., Emeis, K.-C., Hemleben, C., Schulz, H., Sperling, M., Weldeab, S., 2003. Benthic foraminiferal record of ecosystem variability in the eastern Mediterranean Sea during times of sapropel S5 and S6 deposition. Palaeogeogr. Palaeoclimatol. Palaeoecol. 190, 139–164. https://doi.org/10.1016/S0031-0182(02)00603-X

Schmiedl, G., Pfeilsticker, M., Hemleben, C., Mackensen, A., 2004. Environmental and biological effects on the stable isotope composition of recent deep-sea benthic foraminifera from the western Mediterranean Sea. Mar. Micropaleontol. 51, 129–152. https://doi.org/10.1016/J.MARMICRO.2003.10.001

Schroeder, K., Garc\`\ia-Lafuente, J., Josey, S.A., Artale, V., Nardelli, B.B., Carrillo, A., Gacic, M., Gasparini, G. Pietro, Herrmann, M., Lionello, P., others, 2012. Circulation of the Mediterranean Sea and its variability. Clim. Mediterr. Reg. Ed. by Lionello, P., Elsevier 187–256.

Scrivner, A.E., Vance, D., Rohling, E.J., 2004. New neodymium isotope data quantify Nile involvement in Mediterranean anoxic episodes. Geology 32, 565. https://doi.org/10.1130/G20419.1

Shanahan, T.M., McKay, N.P., Hughen, K.A., Overpeck, J.T., Otto-Bliesner, B., Heil, C.W., King, J., Scholz, C.A., Peck, J., 2015. The time-transgressive termination of the African Humid Period. Nat. Geosci. 8, 140–144. https://doi.org/10.1038/ngeo2329

Siddall, M., Khatiwala, S., van de Flierdt, T., Jones, K., Goldstein, S.L., Hemming, S.R., Anderson, R.F., 2008. Towards explaining the Nd paradox using reversible scavenging in an ocean general circulation model. Earth Planet. Sci. Lett. 274, 448–461. https://doi.org/10.1016/j.epsl.2008.07.044

Sierro, F.J., Hodell, D.A., Curtis, J.H., Flores, J.A., Reguera, I., Colmenero-Hidalgo, E., Bárcena, M.A., Grimalt, J.O., Cacho, I., Frigola, J., Canals, M., 2005. Impact of iceberg melting on Mediterranean thermohaline circulation during Heinrich events. Paleoceanography 20, n/a-n/a. https://doi.org/10.1029/2004PA001051

Singh, S.P., Singh, S.K., Goswami, V., Bhushan, R., Rai, V.K., 2012. Spatial distribution of dissolved neodymium and εNd in the Bay of Bengal: Role of particulate matter and mixing of water masses. Geochim. Cosmochim. Acta 94, 38–56. https://doi.org/10.1016/J.GCA.2012.07.017

Skonieczny, C., McGee, D., Winckler, G., Bory, A., Bradtmiller, L.I., Kinsley, C.W., Polissar, P.J., De Pol-Holz, R., Rossignol, L., Malaizé, B., 2019. Monsoon-driven Saharan dust variability over the past 240,000 years. Sci. Adv. 5. https://doi.org/10.1126/sciadv.aav1887

Skonieczny, C., Paillou, P., Bory, A., Bayon, G., Biscara, L., Crosta, X., Eynaud, F., Malaizé, B., Revel, M., Aleman, N., Barusseau, J.P., Vernet, R., Lopez, S., Grousset, F., 2015. African humid periods triggered the reactivation of a large river system in Western Sahara. Nat. Commun. 6.

https://doi.org/10.1038/ncomms9751
Spivack, A.J., Wasserburg, G.J., 1988. Neodymium isotopic composition of the Mediterranean outflow and the eastern North Atlantic. Geochim. Cosmochim. Acta 52, 2767–2773. https://doi.org/10.1016/0016-7037(88)90144-5
Sprovieri, M., Di Stefano, E., Incarbona, A., Salvagio Manta, D., Pelosi, N., Ribera d'Alcalà, M., Sprovieri, R., 2012. Centennial- to millennial-scale climate oscillations in the Central-Eastern Mediterranean Sea between 20,000 and 70,000 years ago: evidence from a high-resolution geochemical and micropaleontological record. Quat. Sci. Rev. 46, 126–135. https://doi.org/10.1016/J.QUASCIREV.2012.05.005
Stratford, K., Williams, R.G., Myers, P.G., 2000. Impact of the circulation on sapropel formation in the eastern Mediterranean. Global Biogeochemical Cycles 14, 683–695.
Tachikawa, K., Athias, V., Jeandel, C., 2003. Neodymium budget in the modern ocean and paleo-oceanographic implications. J. Geophys. Res. 108, 3254. https://doi.org/10.1029/1999JC000285
Tachikawa, K., Piotrowski, A.M., Bayon, G., 2014. Neodymium associated with foraminiferal carbonate as a recorder of seawater isotopic signatures. Quat. Sci. Rev. 88, 1–13. https://doi.org/10.1016/j.quascirev.2013.12.027
Tachikawa, K., Roy-Barman, M., Michard, A., Thouron, D., Yeghicheyan, D., Jeandel, C., 2004. Neodymium isotopes in the Mediterranean Sea: comparison between seawater and sediment signals. Geochim. Cosmochim. Acta 68, 3095–3106. https://doi.org/10.1016/j.gca.2004.01.024
Tachikawa, K., Toyofuku, T., Basile-Doelsch, I., Delhaye, T., 2013. Microscale neodymium distribution in sedimentary planktonic foraminiferal tests and associated mineral phases. Geochim. Cosmochim. Acta 100, 11–23. https://doi.org/10.1016/j.gca.2012.10.010
Tachikawa, K., Vidal, L., Cornuault, M., Garcia, M., Pothin, A., Sonzogni, C., Bard, E., Menot, G., Revel, M., 2015. Eastern Mediterranean Sea circulation inferred from the conditions of S1 sapropel deposition. Clim. Past 11, 855–867. https://doi.org/10.5194/cp-11-855-2015
Tesi, T., Asioli, A., Minisini, D., Maselli, V., Valle, G.D., Gamberi, F., Langone, L., Cattaneo, A., Montagna, P., Trincardi, F., 2017. Large-scale response of the Eastern Mediterranean thermohaline circulation to African monsoon intensification during sapropel S1 formation. Quaternary Science Reviews 159, 139–154.
Thunell, R.C., Williams, D.F., 1989. Glacial–Holocene salinity changes in the Mediterranean Sea: hydrographic and depositional effects. Nature 338, 493–496. https://doi.org/10.1038/338493a0
Toucanne, S., Jouet, G., Ducassou, E., Bassetti, M.A., Dennielou, B., Angue Minto'o, C.M., Lahmi, M., Touyet, N., Charlier, K., Lericolais, G., Mulder, T., 2012. A 130,000-year record of Levantine Intermediate Water flow variability in the Corsica Trough, western Mediterranean Sea. Quat. Sci. Rev. 33, 55–73. https://doi.org/10.1016/j.quascirev.2011.11.020
Toucanne, S., Mintoo, C.M.A., Fontanier, C., Bassetti, M.A., Jorry, S.J., Jouet, G., 2015. Tracking rainfall in the northern Mediterranean borderlands during sapropel deposition. Quaternary Science Reviews 129, 178–195.
Vadsaria, T., Ramstein, G., Dutay, J. -C., Li, L., Ayache, M., Richon, C., 2019. Simulating the Occurrence of the Last Sapropel Event (S1): Mediterranean Basin Ocean Dynamics Simulations Using Nd Isotopic Composition Modeling. Paleoceanogr. Paleoclimatology 34, 237–251. https://doi.org/10.1029/2019PA003566
Vance, D., Burton, K.W., 1999. Neodymium isotopes in planktonic foraminifera: a record of the response of continental weathering and ocean circulation rates to climate change. Earth Planet. Sci. Lett. 173, 365–379. https://doi.org/10.1016/S0012-821X(99)00244-7

Vance, D., Scrivner, A.E., Beney, P., 2004. The use of foraminifera as a record of the past neodymium isotope composition of seawater. Paleoceanography 19, PA2009–PA2009. https://doi.org/10.1029/2003PA000957

Wehausen, R., Brumsack, H.-J., 1999. Cyclic variations in the chemical composition of eastern Mediterranean Pliocene sediments: a key for understanding sapropel formation. Mar. Geol. 153, 161–176. https://doi.org/10.1016/S0025-3227(98)00083-8

Weldeab, S., Emeis, K.-C., Hemleben, C., Siebel, W., 2002a. Provenance of lithogenic surface sediments and pathways of riverine suspended matter in the Eastern Mediterranean Sea: evidence from 143Nd/144Nd and 87Sr/86Sr ratios. Chem. Geol. 186, 139–149. https://doi.org/10.1016/S0009-2541(01)00415-6

Weldeab, S., Emeis, K.-C., Hemleben, C., Vennemann, T.W., Schulz, H., 2002b. Sr and Nd isotope composition of Late Pleistocene sapropels and nonsapropelic sediments from the Eastern Mediterranean Sea: implications for detrital influx and climatic conditions in the source areas. Geochim. Cosmochim. Acta 66, 3585–3598. https://doi.org/10.1016/S0016-7037(02)00954-7

Williams, M.A.., Adamson, D., Cock, B., McEvedy, R., 2000. Late Quaternary environments in the White Nile region, Sudan. Glob. Planet. Change 26, 305–316. https://doi.org/10.1016/S0921-8181(00)00047-3

Wu, J., Böning, P., Pahnke, K., Tachikawa, K., de Lange, G.J., 2016. Unraveling North-African riverine and eolian contributions to central Mediterranean sediments during Holocene sapropel S1 formation. Quat. Sci. Rev. 152, 31–48. https://doi.org/10.1016/J.QUASCIREV.2016.09.029

Wu, J., Liu, Z., Stuut, J.-B. Zhao, Y., Schirone, A., Lange G.-J., 2017. North-African paleodrainage discharges to the central Mediterranean during the last 18,000 years: A multiproxy characterization, Quaternary Science Reviews 163, 95-113

Wu, J., Pahnke, K., Böning, P., Wu, L., Michard, A., de Lange, G.J., 2019. Divergent Mediterranean seawater circulation during Holocene sapropel formation – Reconstructed using Nd isotopes in fish debris and foraminifera. Earth Planet. Sci. Lett. 511, 141–153. https://doi.org/10.1016/J.EPSL.2019.01.036

Wu, Q., Colin, C., Liu, Z., Douville, E., Dubois-Dauphin, Q., Frank, N., 2015a. New insights into hydrological exchange between the South China Sea and the Western Pacific Ocean based on the Nd isotopic composition of seawater. Deep Sea Res. Part II Top. Stud. Oceanogr. 122, 25–40. https://doi.org/10.1016/j.dsr2.2015.11.005

Wu, Q., Colin, C., Liu, Z., Thil, F., Dubois-Dauphin, Q., Frank, N., Tachikawa, K., Bordier, L., Douville, E., 2015b. Neodymium isotopic composition in foraminifera and authigenic phases of the South China Sea sediments: Implications for the hydrology of the North Pacific Ocean over the past 25 kyr. Geochemistry, Geophys. Geosystems 16, 3883–3904. https://doi.org/10.1002/2015GC005871

Xu, Z., Li, T., Colin, C., Clift, P.D., Sun, R., Yu, Z., Wan, S., Lim, D., 2018. Seasonal Variations in the Siliciclastic Fluxes to the Western Philippine Sea and Their Impacts on Seawater ε_{Nd} Values Inferred From 1 Year of In Situ Observations Above Benham Rise. J. Geophys. Res. Ocean. 123, 6688–6702. https://doi.org/10.1029/2018JC014274

Yu, Z., Colin, C., Ma, R., Meynadier, L., Wan, S., Wu, Q., Kallel, N., Sepulcre, S., Dapoigny, A., Bassinot, F., 2018. Antarctic Intermediate Water penetration into the Northern Indian Ocean during the last deglaciation. Earth Planet. Sci. Lett. 500, 67–75. https://doi.org/10.1016/J.EPSL.2018.08.006

Zhao, Y., Colin, C., Liu, Z., Paterne, M., Siani, G., Xie, X., 2012. Reconstructing precipitation changes in northeastern Africa during the Quaternary by clay mineralogical and geochemical investigations of Nile deep-sea fan sediments. Quat. Sci. Rev. 57, 58–70.

https://doi.org/10.1016/J.QUASCIREV.2012.10.009
Zhao, Y., Liu, Z., Colin, C., Paterne, M., Siani, G., Cheng, X., Duchamp-Alphonse, S., Xie, X., 2011. Variations of the Nile suspended discharges during the last 1.75 Myr. Palaeogeogr. Palaeoclimatol. Palaeoecol. 311, 230–241. https://doi.org/10.1016/J.PALAEO.2011.09.001

Depth (cm)	Age (cal kyr BP)	$^{143}Nd/^{144}Nd$	± 2σ	εNd	± 2σ	Samples
0.5	0.7	0.512432	±0.000008	-4.03	± 0.17	uncleaned mixed planktonic foraminifera
2.5	1.3	0.512399	±0.000008	-4.67	± 0.16	uncleaned mixed planktonic foraminifera
6	2.4	0.512345	±0.000007	-5.71	± 0.13	cleaned mixed planktonic foraminifera
6	2.4	0.512351	±0.000007	-5.61	± 0.13	cleaned *G. ruber*
6	2.4	0.512332	±0.000018	-5.97	± 0.35	cleaning solution, mixed planktonic foraminifera
6	2.4	0.512335	±0.000008	-5.91	± 0.15	uncleaned mixed planktonic foraminifera
9.5	3.0	0.512354	±0.000010	-5.53	± 0.20	uncleaned mixed planktonic foraminifera
10	3.1	0.512357	±0.000008	-5.49	± 0.16	cleaned mixed planktonic foraminifera
10	3.1	0.512360	±0.000012	-5.42	± 0.23	uncleaned mixed planktonic foraminifera
10	3.1	0.512359	±0.000007	-5.44	± 0.13	uncleaned mixed planktonic foraminifera
14.5	4.3	0.512358	±0.000009	-5.46	± 0.18	uncleaned mixed planktonic foraminifera
18	5.1	0.512415	±0.000014	-4.36	± 0.27	uncleaned mixed planktonic foraminifera
18	5.1	0.512430	±0.000013	-4.06	± 0.25	uncleaned *G. ruber*
22	5.9	0.512417	±0.000009	-4.31	± 0.18	uncleaned mixed planktonic foraminifera
29	6.9	0.512455	±0.000011	-3.57	± 0.22	uncleaned *G. ruber*
95	8.7	0.512450	±0.000012	-3.67	± 0.23	uncleaned mixed planktonic foraminifera
102	8.9	0.512471	±0.000017	-3.26	± 0.33	uncleaned mixed planktonic foraminifera
102	8.9	0.512490	±0.000015	-2.89	± 0.29	uncleaned *G. ruber*
120	9.1	0.512468	±0.000009	-3.31	± 0.17	uncleaned mixed planktonic foraminifera
200	9.7	0.512498	±0.000009	-2.72	± 0.18	uncleaned mixed planktonic foraminifera
205	9.8	0.512509	±0.000011	-2.51	± 0.21	cleaned mixed planktonic foraminifera
205	9.8	0.512529	±0.000008	-2.12	± 0.16	cleaning solution, mixed planktonic foraminifera
273	12.3	0.512452	±0.000012	-3.63	± 0.23	uncleaned mixed planktonic foraminifera
280	12.7	0.512482	±0.000013	-3.05	± 0.25	uncleaned mixed planktonic foraminifera
293	14.1	0.512450	±0.000009	-3.66	± 0.17	cleaned mixed planktonic foraminifera
293	14.1	0.512474	±0.000007	-3.20	± 0.14	cleaned G. ruber
293	14.1	0.512459	±0.000023	-3.49	± 0.44	cleaning solution, mixed planktonic foraminifera
293	14.1	0.512483	±0.000017	-3.02	± 0.34	cleaning solution, *G. ruber*
299	16.4	0.512398	±0.000010	-4.68	± 0.19	uncleaned mixed planktonic foraminifera
303	20.6	0.512390	±0.000007	-4.83	± 0.14	cleaned mixed planktonic foraminifera
303	20.6	0.512386	±0.000007	-4.91	± 0.14	cleaned mixed planktonic foraminifera
315	25.8	0.512411	±0.000007	-4.44	± 0.13	cleaned G. ruber

Table 1

Depth (cm)	Age (kyr)	$^{143}Nd/^{144}Nd$	± 2σ	εNd	± 2σ
4	0.5	0.512441	±0.000011	-3.84	± 0.21
8	0.9	0.512413	±0.000009	-4.39	± 0.18
16	1.9	0.512410	±0.000008	-4.45	± 0.17
28	3.3	0.512410	±0.000011	-4.45	± 0.21
40	4.7	0.512438	±0.000010	-3.89	± 0.19
52	6.2	0.512454	±0.000010	-3.58	± 0.19
72	8.5	0.512450	±0.000011	-3.66	± 0.22
80	9.5	0.512457	±0.000009	-3.53	± 0.18
108	13.2	0.512476	±0.000009	-3.17	± 0.18
128	15.8	0.512430	±0.000010	-4.07	± 0.19
152	19.0	0.512464	±0.000009	-3.40	± 0.18
160	20.0	0.512462	±0.000010	-3.43	± 0.19
172	22.8	0.512537	±0.000009	-1.96	± 0.17
200	29.5	0.512470	±0.000008	-3.27	± 0.15
224	35.2	0.512483	±0.000008	-3.03	± 0.16
236	38.0	0.512462	±0.000010	-3.43	± 0.19
280	45.0	0.512478	±0.000010	-3.12	± 0.19
304	48.8	0.512474	±0.000010	-3.20	± 0.20
324	51.9	0.512473	±0.000009	-3.22	± 0.18
380	60.8	0.512497	±0.000011	-2.75	± 0.21
384	61.4	0.512483	±0.000009	-3.02	± 0.18
420	67.1	0.512484	±0.000010	-3.00	± 0.19
452	72.1	0.512442	±0.000010	-3.82	± 0.20
484	77.2	0.512430	±0.000010	-4.06	± 0.20
504	80.4	0.512440	±0.000008	-3.85	± 0.16
512	81.8	0.512456	±0.000007	-3.55	± 0.15
524	84.3	0.512459	±0.000008	-3.50	± 0.16
556	91.0	0.512412	±0.000008	-4.42	± 0.15
580	96.0	0.512453	±0.000010	-3.60	± 0.20
592	98.5	0.512455	±0.000009	-3.58	± 0.18
596	99.3	0.512484	±0.000010	-3.00	± 0.19
600	100.2	0.512462	±0.000011	-3.42	± 0.22
604	101.0	0.512469	±0.000009	-3.30	± 0.18
608	102.3	0.512495	±0.000015	-2.79	± 0.29
628	108.7	0.512439	±0.000009	-3.88	± 0.17
632	110.0	0.512331	±0.000008	-5.99	± 0.39
636	110.9	0.512454	±0.000009	-3.59	± 0.16
652	114.5	0.512431	±0.000016	-4.03	± 0.18
656	115.4	0.512432	±0.000010	-4.01	± 0.32
660	116.3	0.512421	±0.000009	-4.23	± 0.19
664	117.2	0.512427	±0.000008	-4.12	± 0.17
668	118.1	0.512415	±0.000009	-4.35	± 0.16

672	119.0	0.512397	±0.000010	-4.70	± 0.17
676	119.9	0.512420	±0.000010	-4.25	± 0.20
680	120.8	0.512405	±0.000011	-4.54	± 0.20
684	121.7	0.512429	±0.000009	-4.07	± 0.22
688	122.6	0.512436	±0.000009	-3.94	± 0.17
692	123.5	0.512429	±0.000013	-4.07	± 0.18
700	128.0	0.512399	±0.000011	-4.66	± 0.24
704	130.3	0.512421	±0.000009	-4.23	± 0.21
708	132.5	0.512418	±0.000012	-4.29	± 0.18
712	134.8	0.512446	±0.000013	-3.75	± 0.23
716	137.0	0.512483	±0.000008	-3.02	± 0.26
720	139.8	0.512448	±0.000009	-3.71	± 0.16
728	145.4	0.512454	±0.000011	-3.59	± 0.17

Table 2

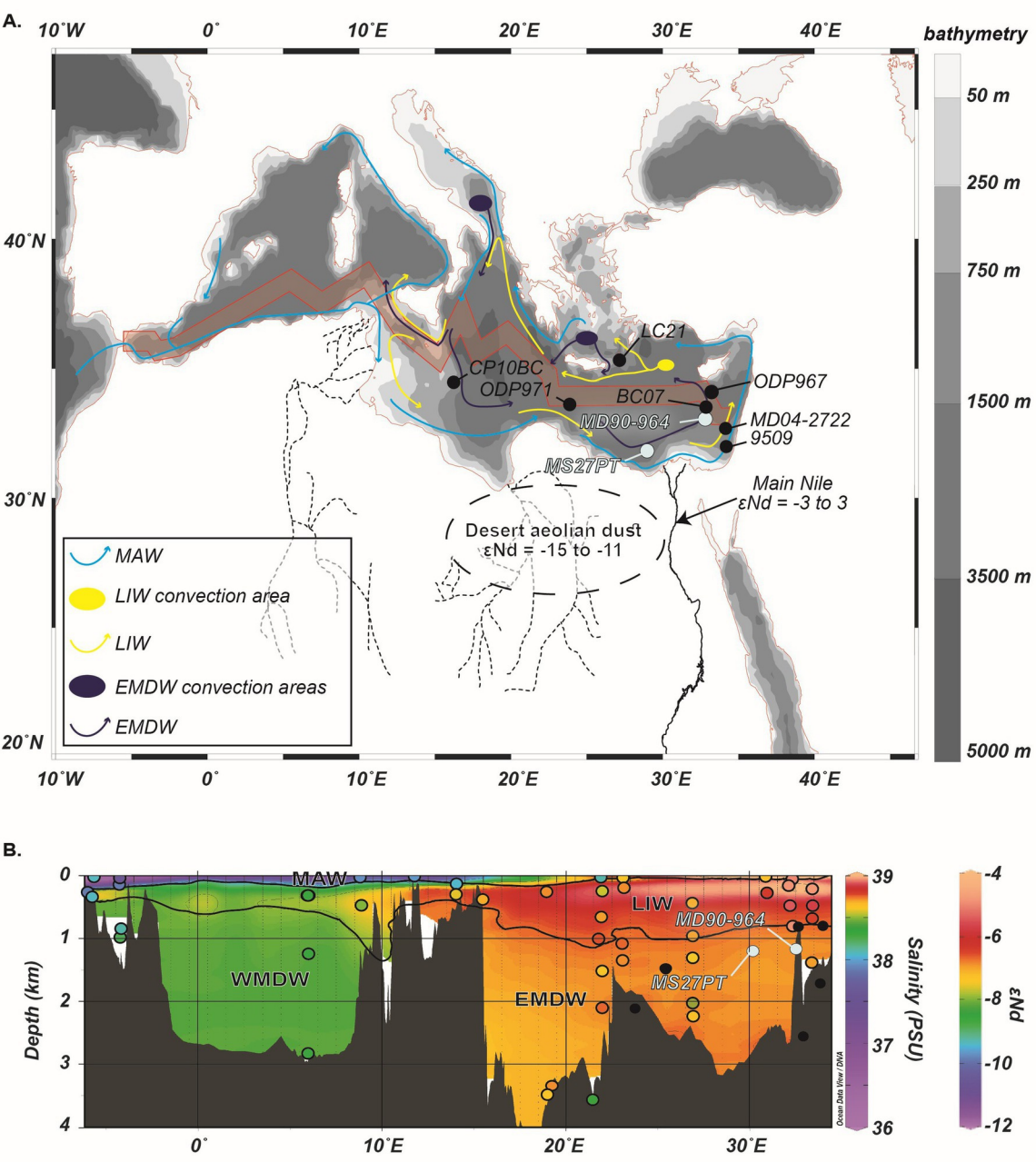
A.
10°W
0°
10°E
20°E
30°E
40°E
40°N
30°N
20°N
bathymetry
50 m
250 m
750 m
1500 m
3500 m
5000 m
LC21
CP10BC
ODP971
ODP967
BC07
MD90-964
MD04-2722
9509
MS27PT
Main Nile
εNd = -3 to 3
Desert aeolian dust
εNd = -15 to -11
MAW
LIW convection area
LIW
EMDW convection areas
EMDW
B.
Depth (km)
0
1
2
3
4
MAW
LIW
MD90-964
WMDW
EMDW
MS27PT
0°
10°E
20°E
30°E
39
38
37
36
Salinity (PSU)
Ocean Data View / DIVA
-4
-6
-8
-10
-12
εNd

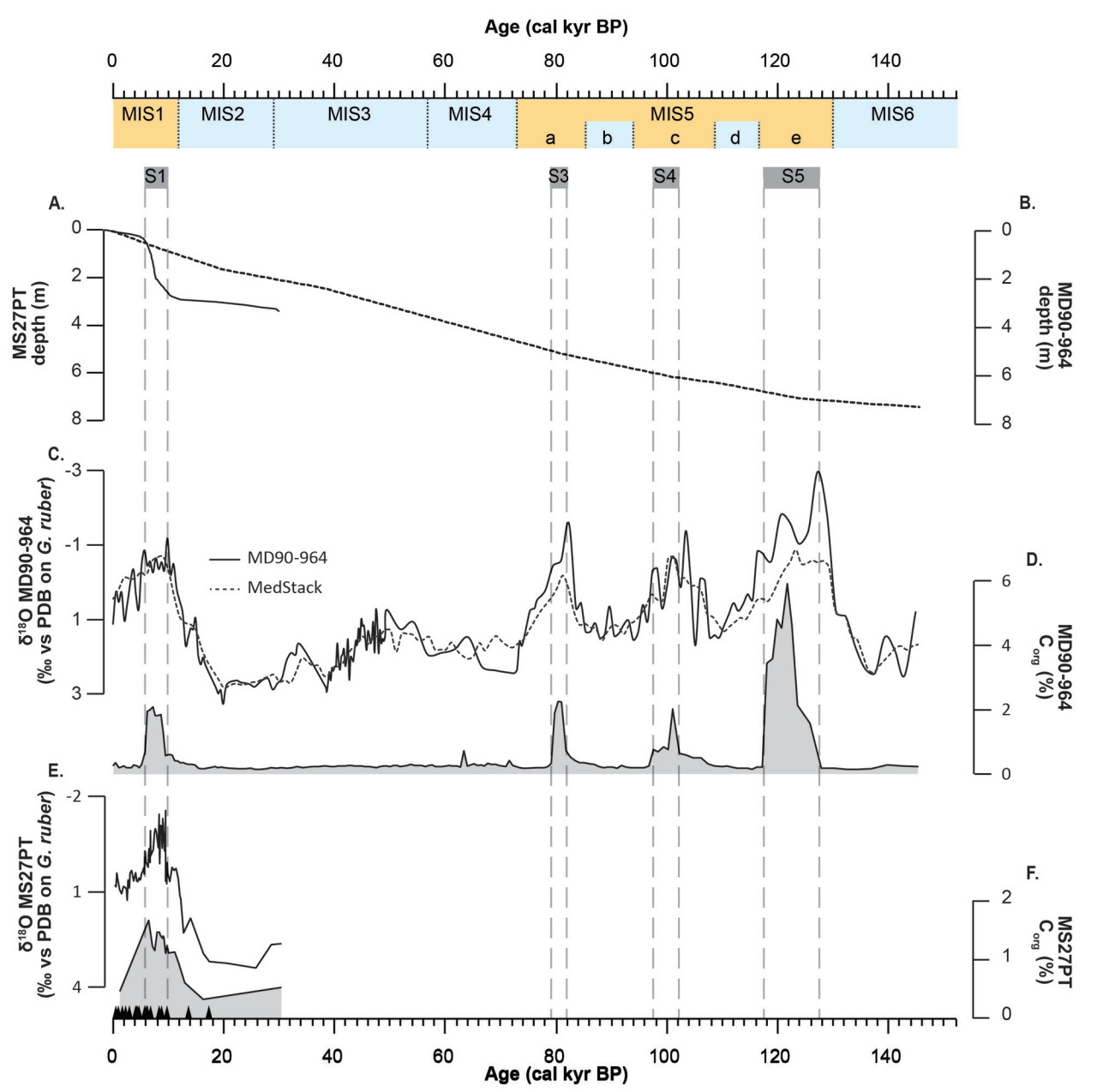
Age (cal kyr BP)
0
20
40
60
80
100
120
140
MIS1
MIS2
MIS3
MIS4
MIS5
a
b
c
d
e
MIS6
S1
S3
S4
S5
A.
B.
C.
D.
E.
F.
MS27PT depth (m)
MD90-964 depth (m)
δ18O MD90-964 (‰ vs PDB on G. ruber)
MD90-964
MedStack
MD90-964 Corg (%)
δ18O MS27PT (‰ vs PDB on G. ruber)
MS27PT Corg (%)
Age (cal kyr BP)

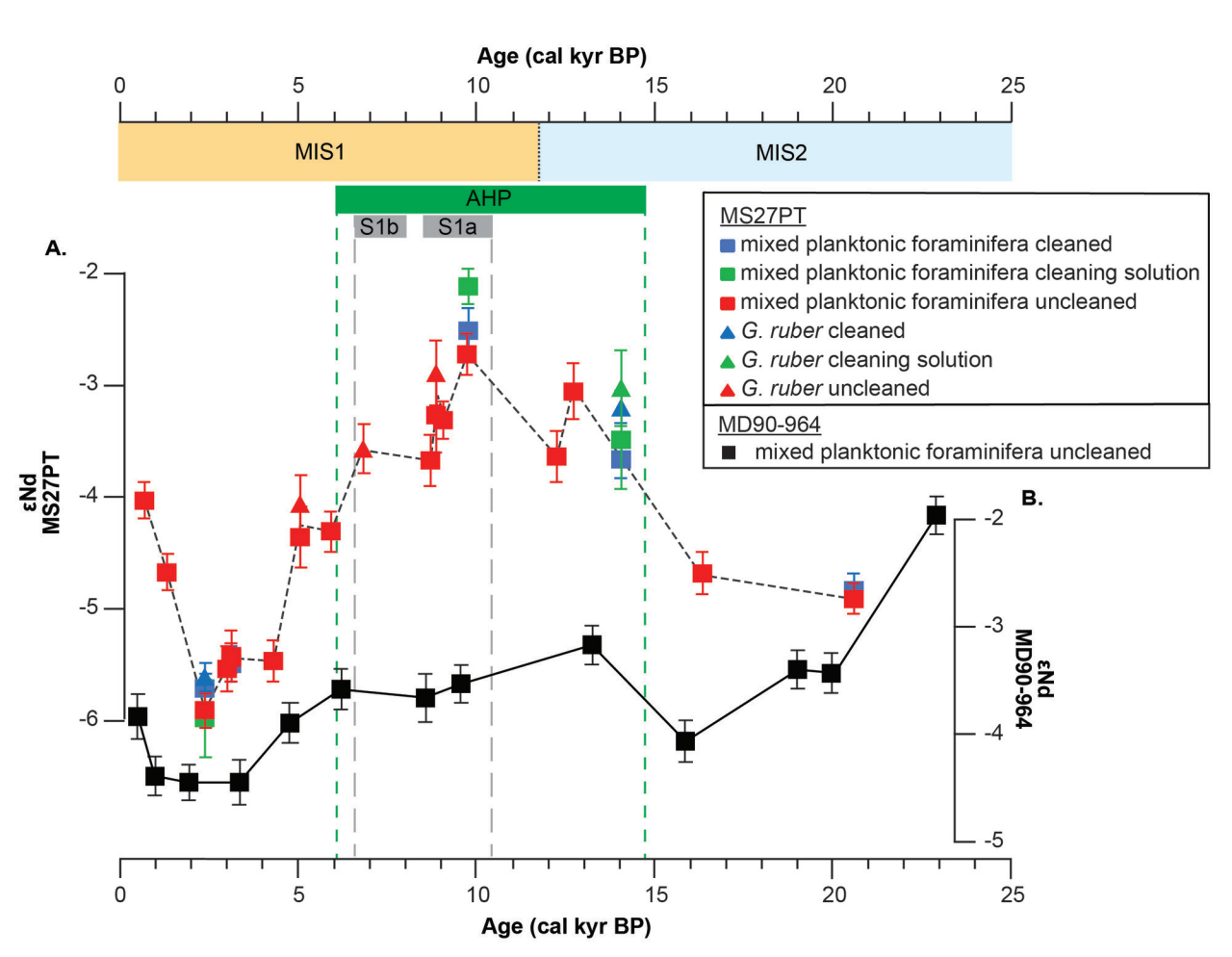
Age (cal kyr BP)
0
5
10
15
20
25
MIS1
MIS2
AHP
S1b
S1a
A.
B.
MS27PT
mixed planktonic foraminifera cleaned
mixed planktonic foraminifera cleaning solution
mixed planktonic foraminifera uncleaned
G. ruber cleaned
G. ruber cleaning solution
G. ruber uncleaned
MD90-964
mixed planktonic foraminifera uncleaned
εNd MS27PT
εNd MD90-964
-2
-3
-4
-5
-6
Age (cal kyr BP)

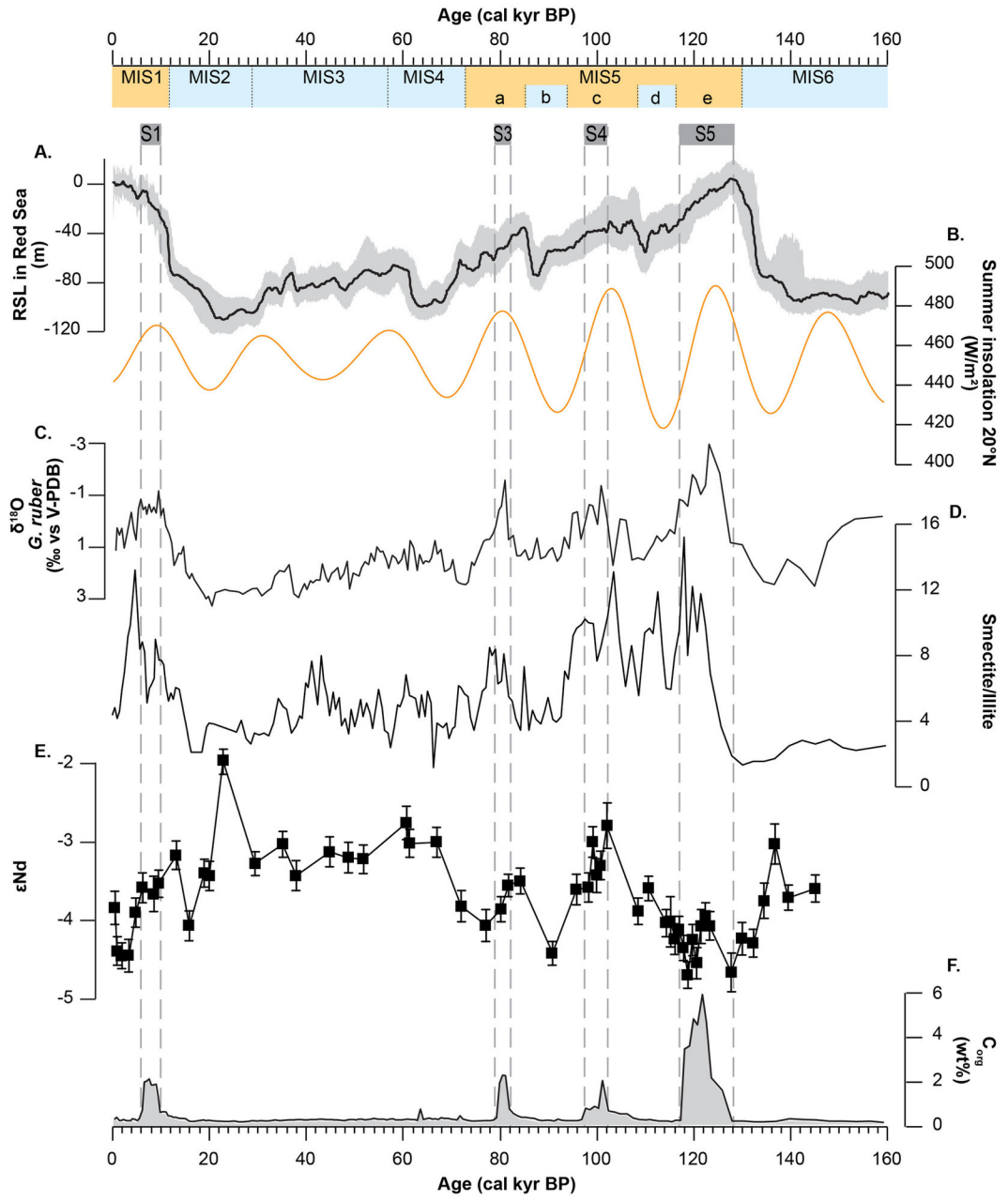
Age (cal kyr BP)
0
20
40
60
80
100
120
140
160
MIS1
MIS2
MIS3
MIS4
MIS5
a
b
c
d
e
MIS6
S1
S3
S4
S5
A.
RSL in Red Sea (m)
0
-40
-80
-120
B.
Summer insolation 20°N (W/m²)
500
480
460
440
420
400
C.
δ18O G. ruber (‰ vs V-PDB)
-3
-1
1
3
D.
Smectite/Illite
16
12
8
4
0
E.
εNd
-2
-3
-4
-5
F.
Corg (wt%)
6
4
2
0
Age (cal kyr BP)

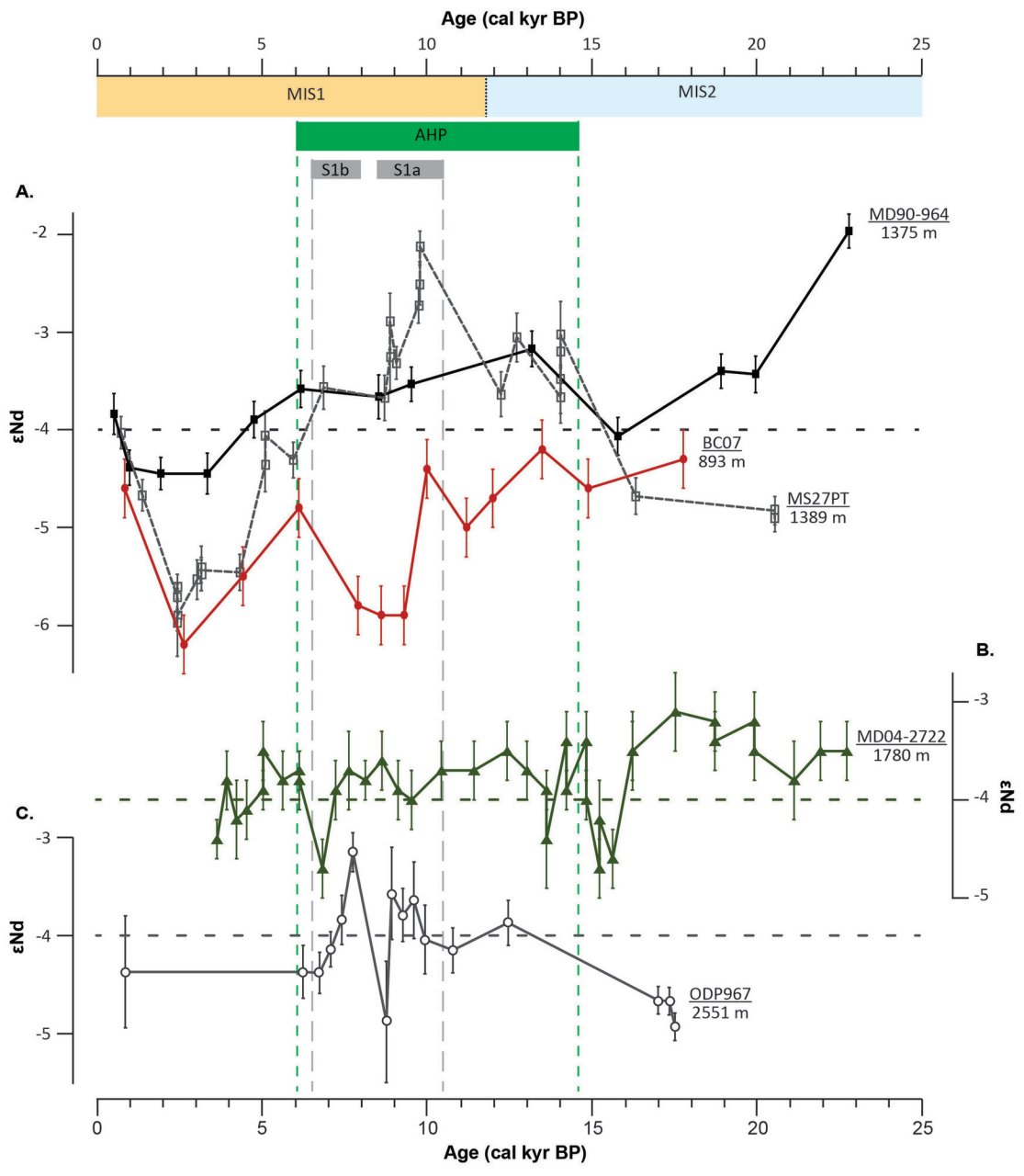
Age (cal kyr BP)
0
5
10
15
20
25
MIS1
MIS2
AHP
S1b
S1a
A.
εNd
-2
-3
-4
-5
-6
MD90-964
1375 m
BC07
893 m
MS27PT
1389 m
B.
MD04-2722
1780 m
εNd³
-3
-4
-5
C.
εNd
-3
-4
-5
ODP967
2551 m
0
5
10
15
20
25
Age (cal kyr BP)

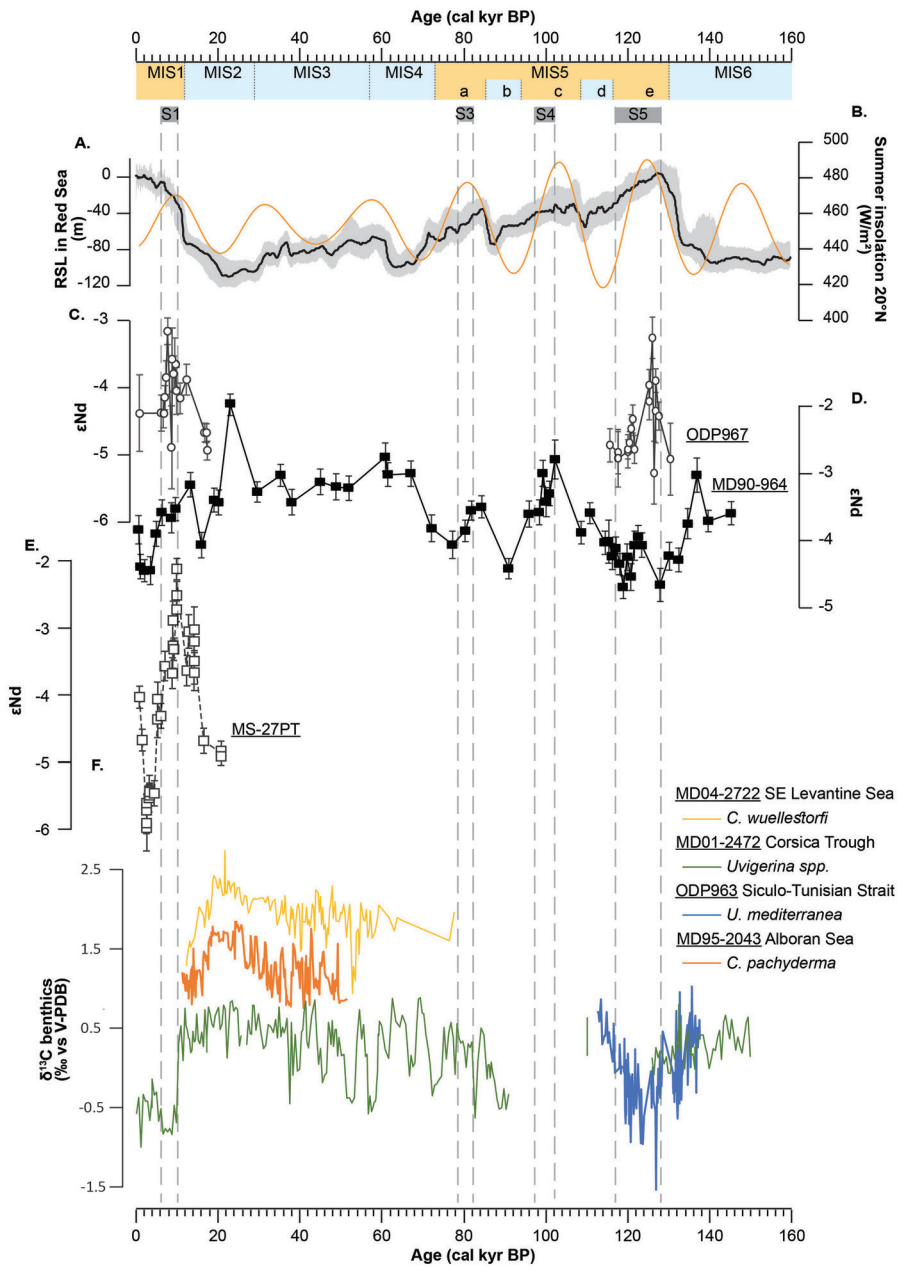
Age (cal kyr BP)
0
20
40
60
80
100
120
140
160
MIS1
MIS2
MIS3
MIS4
MIS5
a
b
c
d
e
MIS6
S1
S3
S4
S5
A.
B.
RSL in Red Sea (m)
0
-40
-80
-120
Summer insolation 20°N (W/m²)
500
480
460
440
420
400
C.
D.
εNd
-3
-4
-5
-6
-2
ODP967
MD90-964
E.
MS-27PT
F.
MD04-2722 SE Levantine Sea
C. wuellestorfi
MD01-2472 Corsica Trough
Uvigerina spp.
ODP963 Siculo-Tunisian Strait
U. mediterranea
MD95-2043 Alboran Sea
C. pachyderma
δ13C benthics (‰ vs V-PDB)
2.5
1.5
0.5
-0.5
-1.5
Age (cal kyr BP)